This article has been accepted for publication in a future issue of this journal, but has not been fully edited. Content may change prior to final publication. Citation information: DOI 10.1109/TWC.2017.2696947, IEEE Transactions on Wireless Communications

In-phase and Quadrature Timing Mismatch Estimation and Compensation in Millimeter-wave Communication Systems

Hlaing Minn, *Fellow, IEEE,* Qi Zhan, *Student Member, IEEE,*
Naofal Al-Dhahir, *Fellow, IEEE,* Huang Huang, *Member, IEEE*

***Abstract*—The emerging millimeter-wave MIMO systems are subject to strong radio frequency (RF) distortions and their compensation is crucial to realize such systems. In the existing literature, several estimation and compensation schemes have been proposed for RF distortions such as carrier frequency offset, phase noise and in-phase and quadrature amplitude and phase imbalance (IQI). However, in-phase and quadrature timing mismatch (IQTM) is largely ignored. This paper investigates the effect of IQTM on millimeter-wave system performance and reveals that IQTM causes a specific image rejection ratio characteristic which is substantially different from the regular frequency-dependent IQI and it substantially prolongs the effective channel length. If not compensated, IQTM can degrade system performance significantly. As a solution to this IQTM problem, this paper proposes novel pilot designs for transmit and receive IQTM estimation, and develops corresponding estimators, transmission protocol and compensation schemes. MIMO averaging is also proposed which substantially enhances the IQTM estimation performance. Simulation results show that our proposed pilot designs and estimators offer an efficient solution to the IQTM problem.**

***Index Terms*—Estimation, IQ timing mismatch, Millimeter-wave, Pilot designs, RF distortions**

I. Introduction

Millimeter-wave (mm-wave) wireless communication systems are gaining increased interest [1]–[3] but they are subject to strong RF distortions. Due to CMOS process variations and the very high sampling frequency used in the mm-wave regime, the difference in signal propagation and processing times of the circuits between the in-phase and quadrature parts of the signal could be significant relative to the sampling interval. This leads to a timing (delay) mismatch between the in-phase and quadrature paths, which we term in-phase and quadrature timing mismatch (IQTM), at both the transmitter (TX) and receiver (RX). IQTM is negligible relative to the sampling interval for systems with carrier frequency below 6 GHz but it becomes significant and can substantially affect the system performance for the emerging mm-wave systems. Not only CMOS process variations, but also device aging and harsh operating conditions could introduce/change IQTMs. Thus, online estimation and compensation of IQTMs is an important open problem, especially for systems operating in the mm-wave band and above.

Related Works: RF distortions constitute important practical problems and most of the related works in the literature consider in-phase and quadrature amplitude and phase imbalance (IQI), phase noise (PN), and carrier frequency offset (CFO). Regarding IQI, [4]–[6] developed blind compensation schemes for RX frequency-dependent IQI in single antenna systems but they require a large number of samples and/or iterations to compute statistics and hence would not be suitable for packet-based transmissions. The TX frequency-dependent IQI calibration was addressed in [7] but its use of a feedback circuitry with analog-to-digital converter would not be appropriate for massive MIMO systems. For multiuser scenarios, [8] assessed performance of TX frequency-independent IQI compensation in OFDMA systems by assuming perfect knowledge of channel and IQI parameters while [9] evaluated symbol error rate performance of a joint compensation and data detection approach by assuming perfect knowledge of RX signal correlation matrices which are functions of the channel and TX and RX frequency-dependent IQI parameters. Pilot-based IQI estimation/compensation schemes were developed in [10]–[12]. Pilot designs for IQI or combined effects of IQI and channels were presented in [13]–[17]. Some works addressed a few RF distortions jointly, e.g., PN plus CFO [20], PN plus IQI [18], [19] and CFO plus IQI [21], [22], [25]. Capacity or mutual information analysis was considered for systems with IQI in [23], PN in [24], IQI and CFO in [25], and PN and IQI in [26]. We note that the above IQI compensation schemes would not work well under much stronger PN levels as experienced in mm-wave systems. Furthermore, in all of the above works, IQTM issue has not been considered. As will be shown in the paper, IQTMs introduce additional cascaded frequency-dependent IQIs whose image rejection ratio (IRR) characteristics are substantially different from those of the regular IQI. Furthermore, IQTMs cause substantial prolonging of the effective channel length, thus requiring substantially larger overhead if pilots are used to estimate the combined effects of IQTM, IQI, and channels. Such pilot overhead increase will be avoided if IQTMs can be (pre)-compensated. These facts highlight the need for separate IQTM estimation/compensation.

To the best of our knowledge, there are only a couple of existing works [27] [28] which are related to IQTMs.

Q. Zhan, H. Minn and N. Al-Dhahir are with the Department of Electrical & Computer Engineering, University of Texas at Dallas, Richardson, TX, USA (Email: {qxz110230, hlaing.minn, aldhahir}@utdallas.edu). H. Huang is with Huawei Technologies Co., Ltd., Shenzhen, China (Email: huanghuang@huawei.com).

This work is partially supported by Huawei Technologies Co., Ltd.
Parts of this work was presented at a Globecom workshop [30].

This article has been accepted for publication in a future issue of this journal, but has not been fully edited. Content may change prior to final publication. Citation information: DOI 10.1109/TWC.2017.2696947, IEEE Transactions on Wireless Communications

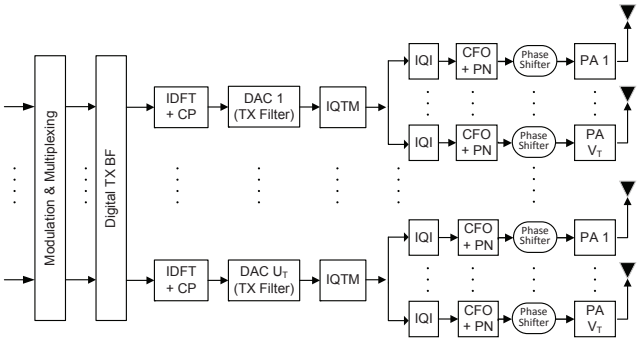

Fig. 1. TX-side signal model block diagram with RF impairments. (BF = beam-forming, PA = power amplifier)

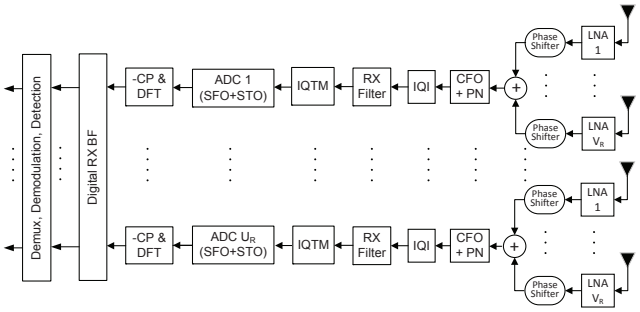

Fig. 2. RX-side signal model block diagram with RF impairments. (LNA = low-noise amplifier)

Reference [27] proposed an IQTM estimation and compensation method for a 4x4 MIMO-OFDM system while [28] just evaluated IQTM's effects on the performance of an optical communication system. Both [27] and [28] consider RX IQTM only; thus, they are not applicable to systems with TX IQTMs. Furthermore, other RF distortions such as PN and CFO were not included in their study, which limits the applicability of their methods/results.

Contributions: Our main contributions are i) the development of the signal model for MIMO OFDM with CFO, TX and RX PN, TX and RX frequency-dependent IQI, sampling time offset (STO), sampling frequency offset (SFO), and TX and RX IQTM, ii) revealing the distinct IRR and effective channel length prolonging characteristics of IQTM, iii) pilot designs for IQTM estimation in the presence of other RF distortions, iv) the corresponding IQTM estimators (without needing to estimate/compensate other impairments), v) IQTM (pre)compensation schemes, and vi) protocol for uplink and downlink IQTM compensation. The proposed pilot designs and IQTM estimators offer good estimation performance for mm-wave systems with severe RF distortions.

Organization: Section II presents signal model and Section III illustrates impacts of IQTM. Section IV develops the IQTM estimation metric and Section V develops pilot designs for IQTM estimation. Estimation and compensation of IQTM are described in Section VI. Performance evaluation results are discussed in Section VII. Conclusions are provided in Section VIII.

Notations: $\mathcal{F}\{\cdot\}$ denotes the Fourier transform. For a vector $\mathbf{x}$, diag$\{\mathbf{x}\}$ represents a diagonal matrix with diagonal elements given by $\mathbf{x}$. $\Re\{\mathbf{x}\}$ and $\Im\{\mathbf{x}\}$ denote the real part and imaginary part of $\mathbf{x}$ while $[\mathbf{x}]_{\rm RI} \triangleq [\Re\{\mathbf{x}^T\}, \Im\{\mathbf{x}^T\}]^T$. For a sequence denoted by J, fliplr$\{J\}$ gives a left-to-right flipped version of the sequence and $|J|$ stands for the number of elements in J. $(\cdot)^*$ and $(\cdot)^T$ denote the complex conjugate and the transpose operation while $*$ stands for the convolution. $\mathbf{J}$ is an antidiagonal matrix with all-one antidiagonal elements. We us the following Matlab notations, $k:n = \{k, k+1, k+2, \ldots, n\}$ and $k:m:n = \{k, k+m, k+2m, \ldots, k+lm\}$ where $l = \lfloor (n-k)/m \rfloor$.

II. Signal Model

In this section, we develop the signal model under various RF distortions such as CFO, PN, IQI, SFO, STO, and IQTM. Since the single-carrier frequency domain equalization (SC-FDE) can be viewed as discrete Fourier transform (DFT) precoded OFDM, our signal model will be presented based on OFDM with a DFT size of $N_{\rm DFT}$, subcarrier spacing Δf and $N_{\rm cp}$ cyclic prefix (CP) samples. Fig. 1 and Fig. 2 show the system block diagrams at the TX and the RX, respectively. The TX has U_T digital-to-analog conversion (DAC) branches and each branch is connected to V_T antenna elements. The RX has U_R analog-to-digital conversion (ADC) branches and each branch is connected to V_R antenna elements. The DAC (ADC) branch index is denoted by u_1 (u_2) and the antenna index connected to a DAC (ADC) branch is referred to by v_1 (v_2). Note that IQTMs introduced by DACs/ADCs are absorbed in the IQTM blocks in the figures.

Let $\{c_{u_1,k}\}$ represent the TX IDFT output signal (after CP insertion) for the input frequency-domain symbols $\{C_{u_1}[l]\}$. Denote the TX pulse shape filter impulse response as $g_T(t)$ and the TX sampling period at the output of IDFT as T_s. The filtered OFDM signal at the DAC branch u_1 without IQTM is given by

$$s_{u_1}(t) = \sum_k c_{u_1,k} g_T(t - kT_s) \tag{1}$$

and its Fourier transform $S_{u_1}(f) = \mathcal{F}\{s_{u_1}(t)\}$ reads as

$$S_{u_1}(f) = G_T(f) \sum_{l=0}^{N_{\rm DFT}-1} C_{u_1}[l]\ \gamma_T(f - \frac{l}{N_{\rm DFT} T_s}) \tag{2}$$

where $G_T(f) = \mathcal{F}\{g_T(t)\}$ and $\gamma_T(f)$ is the TX subcarrier filter given by

$$\gamma_T(f) \triangleq \frac{N_{\rm DFT} + N_{\rm cp}}{\sqrt{N_{\rm DFT}}}\ e^{-j\pi T_s f (N_{\rm DFT} - N_{\rm cp} - 1)} \times \frac{\mathrm{sinc}\left(f T_s (N_{\rm DFT} + N_{\rm cp})\right)}{\mathrm{sinc}\left(f T_s\right)}. \tag{3}$$

Note that $\gamma_T(f)$ is periodic with period $1/T_s$, the spectral mainlobe of $\gamma_T(f)$ within a period has a bandwidth of $2/(T_s(N_{\rm DFT} + N_{\rm cp})$ (narrow-band), and $\gamma_T(f) = \gamma_T^*(-f)$.

When there is IQTM at TX, such time mismatch can be modeled by introducing a time delay $\tau_{{\rm tx},u_1}$ to $\Im\{s_{u_1}(t)\}$ with respect to $\Re\{s_{u_1}(t)\}$ (or the reverse order), where $\tau_{\rm tx}$ can take

This article has been accepted for publication in a future issue of this journal, but has not been fully edited. Content may change prior to final publication. Citation information: DOI 10.1109/TWC.2017.2696947, IEEE Transactions on Wireless Communications

either a positive or negative value. With IQTM, the signal at the output of the DAC branch u_1 becomes

$$\breve{s}_{u_1}(t) = \Re\{s_{u_1}(t)\} + j\Im\{s_{u_1}(t-\tau_{\mathrm{tx},u_1})\}. \quad (4)$$

Then, $\breve{S}_{u_1}(f) = \mathcal{F}\{\breve{s}_{u_1}(t)\}$ is given by

$$\breve{S}_{u_1}(f) = S_{u_1}(f)\frac{1+e^{-j2\pi f\tau_{\mathrm{tx},u_1}}}{2} + S^*_{u_1}(-f)\frac{1-e^{-j2\pi f\tau_{\mathrm{tx},u_1}}}{2}. \quad (5)$$

Let a^I_{T,u_1,v_1} and θ^I_{T,u_1,v_1} be the frequency-independent gain and phase of the inphase branch at TX and a^Q_{T,u_1,v_1} and θ^Q_{T,u_1,v_1} be those of the quadrature branch. Let the frequency-dependent gain and phase mismatches be represented by the inphase branch filter $p^I_{T,u_1,v_1}(t)$ and the quadrature branch filter $p^Q_{T,u_1,v_1}(t)$. Then, the (virtual) filters representing TX IQI are given by [16]

$$\begin{aligned}\mu_{T,u_1,v_1}(t) =& 0.5(a^I_{T,u_1,v_1}e^{j\theta^I_{T,u_1,v_1}}p^I_{T,u_1,v_1}(t) \\ &+ a^Q_{T,u_1,v_1}e^{j\theta^Q_{T,u_1,v_1}}p^Q_{T,u_1,v_1}(t)), \quad (6)\\ \nu_{T,u_1,v_1}(t) =& 0.5(a^I_{T,u_1,v_1}e^{j\theta^I_{T,u_1,v_1}}p^I_{T,u_1,v_1}(t) \\ &- a^Q_{T,u_1,v_1}e^{j\theta^Q_{T,u_1,v_1}}p^Q_{T,u_1,v_1}(t)). \quad (7)\end{aligned}$$

Similarly, with the RX IQI parameters a^I_{R,u_2}, θ^I_{R,u_2}, a^Q_{R,u_2}, θ^Q_{R,u_2}, $p^I_{R,u_2}(t)$, and $p^Q_{R,u_2}(t)$, the filters representing RX IQI are [16]

$$\mu_{R,u_2}(t) = \frac{a^I_{R,u_2}e^{-j\theta^I_{R,u_2}}p^I_{R,u_2}(t) + a^Q_{R,u_2}e^{-j\theta^Q_{R,u_2}}p^Q_{R,u_2}(t)}{2}, \quad (8)$$

$$\nu_{R,u_2}(t) = \frac{a^I_{R,u_2}e^{j\theta^I_{R,u_2}}p^I_{R,u_2}(t) - a^Q_{R,u_2}e^{j\theta^Q_{R,u_2}}p^Q_{R,u_2}(t)}{2}. \quad (9)$$

If IQI is frequency-independent, $p^I_{T,u_1,v_1}(t) = p^Q_{T,u_1,v_1}(t) = \delta(t)$ and $p^I_{R,u_2}(t) = p^Q_{R,u_2}(t) = \delta(t)$.

The effects of TX IQI and PN can be modeled by

$$\begin{aligned}x_{u_1,v_1}(t) = e^{j\phi_{T,u_1}(t)}&[\mu_{T,u_1,v_1}(t) * \breve{s}_{u_1}(t) \\ &+ \nu_{T,u_1,v_1}(t) * \breve{s}^*_{u_1}(t)] \quad (10)\end{aligned}$$

where $e^{j\phi_{T,u_1}(t)}$ represents TX PN (+ TX CFO). From (4) and (10), we obtain

$$\begin{aligned}x_{u_1,v_1}(t) = e^{j\phi_{T,u_1}(t)}&[\bar{\mu}_{T,u_1,v_1}(t) * s_{u_1}(t) \\ &+ \bar{\nu}_{T,u_1,v_1}(t) * s^*_{u_1}(t)] \quad (11)\end{aligned}$$

where

$$\begin{aligned}\bar{\mu}_{T,u_1,v_1}(t) =& [\mu_{T,u_1,v_1}(t) + \mu_{T,u_1,v_1}(t-\tau_{\mathrm{tx},u_1}) + \nu_{T,u_1,v_1}(t) \\ &- \nu_{T,u_1,v_1}(t-\tau_{\mathrm{tx},u_1})]/2, \quad (12)\\ \bar{\nu}_{T,u_1,v_1}(t) =& [\mu_{T,u_1,v_1}(t) - \mu_{T,u_1,v_1}(t-\tau_{\mathrm{tx},u_1}) + \nu_{T,u_1,v_1}(t) \\ &+ \nu_{T,u_1,v_1}(t-\tau_{\mathrm{tx},u_1})]/2. \quad (13)\end{aligned}$$

Note that $\bar{\mu}_{T,u_1,v_1}(t)$ and $\bar{\nu}_{T,u_1,v_1}(t)$ represent the cascaded effects of TX IQTM and TX IQI.

The received signal at antenna v_2 in ADC branch u_2 is

$$\begin{aligned}r_{u_2,v_2}(t) = &\sum_{u_1=1}^{U_T}\sum_{v_1=1}^{V_T}\sum_{l=1}^{L} x_{u_1,v_1}(t-\tau_l)e^{j\theta_{T,u_1,v_1}}h^{u_2,v_2}_{u_1,v_1}(t,l) \\ &+ w_{u_2,v_2}(t) \quad (14)\end{aligned}$$

where we assume that each multipath channel has L paths, and $e^{j\theta_{T,u_1,v_1}}$ is the TX analog beamforming coefficient, $h^{u_2,v_2}_{u_1,v_1}(t,l)$ is the lth tap channel coefficient at time t between antenna element v_1 in TX DAC branch u_1 and antenna element v_2 in RX ADC branch u_2, and $w_{u_2,v_2}(t)$ is an additive white Gaussian noise process. Then, after analog beamforming with weights $\{e^{j\theta_{R,u_2,v_2}}\}$ at RX, the signal at the ADC branch u_2 is given by

$$r_{u_2}(t) = \sum_{v_2=1}^{V_R} r_{u_2,v_2}(t)\; e^{j\theta_{R,u_2,v_2}}. \quad (15)$$

Let α_{u_2} denote the CFO, $g_R(t)$ the RX filter impulse response, and $e^{-j\phi_{R,u_2}(t)}$ the RX PN. After experiencing PN, CFO and IQI (c.f. Fig. 2), the signal becomes

$$\begin{aligned}\tilde{y}_{u_2}(t) =& \mu_{R,u_2}(t) * \left(r_{u_2}(t)e^{-j\phi_{R,u_2}(t)}e^{-j2\pi\alpha_{u_2}t}\right) \\ &+ \nu_{R,u_2}(t) * \left(r_{u_2}(t)e^{-j\phi_{R,u_2}(t)}e^{-j2\pi\alpha_{u_2}t}\right)^*. \quad (16)\end{aligned}$$

Next, after passing through the RX filter, the output signal is given by

$$y_{u_2}(t) = \tilde{y}_{u_2}(t) * g_R(t) = \mu_{R,u_2}(t) * \tilde{r}_{u_2}(t) + \nu_{R,u_2}(t) * \tilde{r}^*_{u_2}(t) \quad (17)$$

where

$$\tilde{r}_{u_2}(t) \triangleq (r_{u_2}(t)e^{-j\phi_{R,u_2}(t)}e^{-j2\pi\alpha_{u_2}t}) * g_R(t). \quad (18)$$

Applying the Fourier transform, we have $Y_{u_2}(f) = \mathcal{F}\{y_{u_2}(t)\}$, $\tilde{R}_{u_2}(f) = \mathcal{F}\{\tilde{r}_{u_2}(t)\}$, $\mathcal{M}_{R,u_2}(f) = \mathcal{F}\{\mu_{R,u_2}(t)\}$, $\mathcal{N}_{R,u_2}(f) = \mathcal{F}\{\nu_{R,u_2}(t)\}$ and

$$Y_{u_2}(f) = \mathcal{M}_{R,u_2}(f)\tilde{R}_{u_2}(f) + \mathcal{N}_{R,u_2}(f)\tilde{R}^*_{u_2}(-f). \quad (19)$$

When there is IQTM at RX, such time mismatch can be modeled, in the same manner as in TX IQTM, and the corresponding RX filter output signal is given by

$$\breve{y}_{u_2}(t) = \Re\{y_{u_2}(t)\} + j\Im\{y_{u_2}(t-\tau_{\mathrm{rx},u_2})\}. \quad (20)$$

Then, $\breve{Y}_{u_2}(f) = \mathcal{F}\{\breve{y}_{u_2}(t)\}$ is related to $Y_{u_2}(f)$ by

$$\breve{Y}_{u_2}(f) = Y_{u_2}(f)\frac{1+e^{-j2\pi f\tau_{\mathrm{rx},u_2}}}{2} + Y^*_{u_2}(-f)\frac{1-e^{-j2\pi f\tau_{\mathrm{rx},u_2}}}{2}. \quad (21)$$

From (17) and (20), we obtain

$$\breve{y}_{u_2}(t) = \bar{\mu}_{R,u_2}(t) * \tilde{r}_{u_2}(t) + \bar{\nu}_{R,u_2}(t) * \tilde{r}^*_{u_2}(t) \quad (22)$$

where $\bar{\mu}_{R,u_2}(t)$ and $\bar{\nu}_{R,u_2}(t)$ are equivalent (virtual) IQI filters representing the effects of cascaded RX IQI and RX IQTM and given by

$$\begin{aligned}\bar{\mu}_{R,u_2}(t) =& [\mu_{R,u_2}(t) + \mu_{R,u_2}(t-\tau_{\mathrm{rx},u_2}) + \nu^*_{R,u_2}(t) \\ &- \nu^*_{R,u_2}(t-\tau_{\mathrm{rx},u_2})]/2, \quad (23)\\ \bar{\nu}_{R,u_2}(t) =& [\mu^*_{R,u_2}(t) - \mu^*_{R,u_2}(t-\tau_{\mathrm{rx},u_2}) + \nu_{R,u_2}(t) \\ &+ \nu_{R,u_2}(t-\tau_{\mathrm{rx},u_2})]/2. \quad (24)\end{aligned}$$

This article has been accepted for publication in a future issue of this journal, but has not been fully edited. Content may change prior to final publication. Citation information: DOI 10.1109/TWC.2017.2696947, IEEE Transactions on Wireless Communications

If there is a SFO between the sampling frequencies of TX IDFT and RX DFT, then the RX DFT sampling period T_s' would be different from the TX IDFT sampling period T_s. Furthermore, the RX filter output sampling time instant could deviate from the optimal sampling instant, resulting a STO t_0. The sampled version of (20) is given by $\breve{y}_{u_2}[k] \triangleq \breve{y}_{u_2}(kT_s' + t_0)$. After the CP removal, applying DFT to $\{\breve{y}_{u_2}[k]\}$ of an OFDM symbol yields the frequency-domain received signal on sub-carrier n (i.e., at frequency $f_n \triangleq n/(N_{\rm DFT}T_s')$) as

$$\begin{aligned}\breve{Y}_{u_2}[n] =& \frac{1}{\sqrt{N_{\rm DFT}}} \sum_{k=0}^{N_{\rm DFT}-1} \breve{y}_{u_2}[k] e^{\frac{-j2\pi nk}{N_{\rm DFT}}} \\ =& [(\breve{Y}_{u_2}(f)e^{j2\pi f t_0}) * \gamma_R(f)]_{f=f_n} \end{aligned} \quad (25)$$

where $\gamma_R(f)$ is the RX subcarrier filter given by

$$\gamma_R(f) \triangleq \sqrt{N_{\rm DFT}}\, e^{-j\pi T_s' f(N_{\rm DFT}-1)} \frac{\mathrm{sinc}\,(fT_s'N_{\rm DFT})}{\mathrm{sinc}\,(fT_s')}. \quad (26)$$

$\gamma_R(f)$ is periodic with a period $1/T_s'$, has the mainlobe bandwidth of $2/(T_s'N_{\rm DFT})$ (narrow-band), and $\gamma_R(f) = \gamma_R^*(-f)$.

Define $G_R(f) \triangleq \mathcal{F}\{g_R(t)\}$, $W_{u_2,v_2}(f) = \mathcal{F}\{w_{u_2,v_2}(t)\}$, $W_{u_2}(f) \triangleq \sum_{v_2=1}^{V_R} e^{j\theta_{R,u_2,v_2}} W_{u_2,v_2}(f)$, $H_{u_1,v_1}^{u_2,v_2}(f) \triangleq \mathcal{F}\{h_{u_1,v_1}^{u_2,v_2}(t)\}$, $H_{u_1,v_1}^{u_2}(f) \triangleq \sum_{v_2=1}^{V_R} e^{j\theta_{R,u_2,v_2}} H_{u_1,v_1}^{u_2,v_2}(f)$, $\bar{\mathcal{M}}_{T,u_1,v_1}(f) = \mathcal{F}\{\bar{\mu}_{T,u_1,v_1}(t)\}$, $\bar{\mathcal{N}}_{T,u_1,v_1}(f) = \mathcal{F}\{\bar{\nu}_{T,u_1,v_1}(t)\}$, $\bar{\mathcal{M}}_{R,u_2}(f) = \mathcal{F}\{\bar{\mu}_{R,u_2}(f)\}$, $\bar{\mathcal{N}}_{R,u_2}(f) = \mathcal{F}\{\bar{\nu}_{R,u_2}(f)\}$, $\Psi_{T,u_1}(f) \triangleq \mathcal{F}\{e^{j\phi_{T,u_1}(t)}\mathrm{rec}(t)\}$ and $\Psi_{R,u_2}(f) \triangleq \mathcal{F}\{e^{-j\phi_{R,u_2}(t)}\mathrm{rec}(t)\}$ where $\mathrm{rec}(t)$ is a unit-amplitude rectangular function covering the considered OFDM symbol.

Then, after some manipulation (See Appendix), we can express $\breve{Y}_{u_2}[n]$ as

$$\begin{aligned}\breve{Y}_{u_2}[n] =& \sum_{u_1=1}^{U_T} \sum_{l} \big\{ C_{u_1}[l] \left(A_{u_2,u_1}^{\mu\mu}[n,l] + A_{u_2,u_1}^{\nu\nu}[n,l] \right) \\ &+ C_{u_1}[l]^* \left(A_{u_2,u_1}^{\nu\mu}[n,l] + A_{u_2,u_1}^{\mu\nu}[n,l] \right) \big\} + \breve{\eta}_{u_2}[n] \end{aligned} \quad (27)$$

where $A_{u_2,u_1}^{\mu\mu}[n,l]$, $A_{u_2,u_1}^{\nu\nu}[n,l]$, $A_{u_2,u_1}^{\nu\mu}[n,l]$, and $A_{u_2,u_1}^{\mu\nu}[n,l]$ represent the cross-coupling mechanisms from subcarrier l to subcarrier n due to the effects of TX and RX impairments, the channels, and the analog beamforming, and they are given in (80), (81), (82), and (83), respectively. The noise term $\breve{\eta}_{u_2}[n]$ is given in (84).

Denote the indexes of the used subcarriers by $[k_1, \cdots, k_N]$ where (k_1, k_N), (k_2, k_{N-1}), $\cdots$, $(k_{0.5N}, k_{0.5N+1})$ are mirror pairs. Define $\breve{\mathbf{Y}}_{u_2} = \left[\breve{Y}_{u_2}[k_1], \cdots, \breve{Y}_{u_2}[k_N]\right]^T$, $\mathbf{C}_{u_1} = [C_{u_1}[k_1], \cdots, C_{u_1}[k_N]]^T$, $\breve{\boldsymbol{\eta}}_{u_2} = [\breve{\eta}_{u_2}[k_1], \cdots, \breve{\eta}_{u_2}[k_N]]^T$. Also, define $N \times N$ matrices $\mathbf{A}_{\mathbf{u_2},\mathbf{u_1}}^{\mu\mu}$, $\mathbf{A}_{\mathbf{u_2},\mathbf{u_1}}^{\nu\nu}$, $\mathbf{A}_{\mathbf{u_2},\mathbf{u_1}}^{\nu\mu}$, $\mathbf{A}_{\mathbf{u_2},\mathbf{u_1}}^{\mu\nu}$ such that their (nth row, lth column) elements are given by $A_{u_2,u_1}^{\mu\mu}[k_n,k_l]$, $A_{u_2,u_1}^{\nu\nu}[k_n,k_l]$, $A_{u_2,u_1}^{\nu\mu}[k_n,k_l]$, $A_{u_2,u_1}^{\mu\nu}[k_n,k_l]$, respectively. Then, we can express (27) in a matrix form as

$$\begin{aligned}\breve{\mathbf{Y}}_{u_2} =& \sum_{u_1=1}^{U_T} \{ (\mathbf{A}_{\mathbf{u_2},\mathbf{u_1}}^{\mu\mu} + \mathbf{A}_{\mathbf{u_2},\mathbf{u_1}}^{\nu\nu}) \mathbf{C}_{u_1} \\ &+ (\mathbf{A}_{\mathbf{u_2},\mathbf{u_1}}^{\nu\mu} + \mathbf{A}_{\mathbf{u_2},\mathbf{u_1}}^{\mu\nu}) \mathbf{C}_{u_1}^* \} + \breve{\boldsymbol{\eta}}_{u_2}. \end{aligned} \quad (28)$$

We can also express (28) in a real-valued matrix form as

$$[\breve{\mathbf{Y}}_{u_2}]_{\rm RI} = \sum_{u_1=1}^{U_T} \mathbf{Q}_{u_2,u_1} [\mathbf{C}_{u_1}]_{\rm RI} + [\breve{\boldsymbol{\eta}}_{u_2}]_{\rm RI} \quad (29)$$

where

$$\mathbf{Q}_{u_2,u_1} \triangleq \begin{bmatrix} \Re\{\mathbf{U}_{u_2,u_1}\} & -\Im\{\mathbf{V}_{u_2,u_1}\} \\ \Im\{\mathbf{U}_{u_2,u_1}\} & \Re\{\mathbf{V}_{u_2,u_1}\} \end{bmatrix}, \quad (30)$$

$$\mathbf{U}_{u_2,u_1} \triangleq \mathbf{A}_{\mathbf{u_2},\mathbf{u_1}}^{\mu\mu} + \mathbf{A}_{\mathbf{u_2},\mathbf{u_1}}^{\nu\nu} + \mathbf{A}_{\mathbf{u_2},\mathbf{u_1}}^{\nu\mu} + \mathbf{A}_{\mathbf{u_2},\mathbf{u_1}}^{\mu\nu}, \quad (31)$$

$$\mathbf{V}_{u_2,u_1} \triangleq \mathbf{A}_{\mathbf{u_2},\mathbf{u_1}}^{\mu\mu} + \mathbf{A}_{\mathbf{u_2},\mathbf{u_1}}^{\nu\nu} - \mathbf{A}_{\mathbf{u_2},\mathbf{u_1}}^{\nu\mu} - \mathbf{A}_{\mathbf{u_2},\mathbf{u_1}}^{\mu\nu}. \quad (32)$$

Next, to estimate TX and RX IQTMs, we decouple effects of IQTM from those of other distortions. First, define the following equations (33)-(38):

$$\boldsymbol{\Lambda}_{\rm D}(\tau) \triangleq \mathrm{diag}\Big\{ \frac{1+e^{-j2\pi f_{k_1}\tau}}{2}, \cdots, \frac{1+e^{-j2\pi f_{k_N}\tau}}{2} \Big\} \quad (33)$$

$$\boldsymbol{\Lambda}_{\rm M}(\tau) \triangleq \mathrm{diag}\Big\{ \frac{1-e^{-j2\pi f_{k_1}\tau}}{2}, \cdots, \frac{1-e^{-j2\pi f_{k_N}\tau}}{2} \Big\} \quad (34)$$

$$\boldsymbol{\Lambda}_{\mu_{R,u_2}} \triangleq \mathrm{diag}\left\{ \mathcal{M}_{R,u_2}[k_1], \cdots, \mathcal{M}_{R,u_2}[k_N] \right\} \quad (35)$$

$$\boldsymbol{\Lambda}_{\nu_{R,u_2}} \triangleq \mathrm{diag}\left\{ \mathcal{N}_{R,u_2}[k_1], \cdots, \mathcal{N}_{R,u_2}[k_N] \right\} \quad (36)$$

Let $\mathbf{D}_{u_2,u_1}^{\mu}$ and $\mathbf{D}_{u_2,u_1}^{\nu}$ represent $N \times N$ matrices with (nth row, lth column) elements given by $D_{u_2,u_1}^{\mu}[k_n,k_l]$ in (91) and $D_{u_2,u_1}^{\nu}[k_n,k_l]$ in (92), respectively. Next, define

$$\mathbf{B}_{u_2,u_1}^{D} \triangleq \boldsymbol{\Lambda}_{\mu_{R,u_2}} \mathbf{D}_{u_2,u_1}^{\mu} + \boldsymbol{\Lambda}_{\nu_{R,u_2}} \mathbf{J} \mathbf{D}_{u_2,u_1}^{\nu*} \mathbf{J}, \quad (39)$$

$$\mathbf{B}_{u_2,u_1}^{M} \triangleq \boldsymbol{\Lambda}_{\mu_{R,u_2}} \mathbf{D}_{u_2,u_1}^{\nu} \mathbf{J} + \boldsymbol{\Lambda}_{\nu_{R,u_2}} \mathbf{J} \mathbf{D}_{u_2,u_1}^{\mu*}, \quad (40)$$

$$\bar{\mathbf{Q}}_{u_2,u_1} \triangleq \begin{bmatrix} \Re\{\mathbf{B}_{u_2,u_1}^{D} + \mathbf{B}_{u_2,u_1}^{M}\} & \Im\{\mathbf{B}_{u_2,u_1}^{M} - \mathbf{B}_{u_2,u_1}^{D}\} \\ \Im\{\mathbf{B}_{u_2,u_1}^{D} + \mathbf{B}_{u_2,u_1}^{M}\} & \Re\{\mathbf{B}_{u_2,u_1}^{D} - \mathbf{B}_{u_2,u_1}^{M}\} \end{bmatrix}. \quad (41)$$

Then, after some manipulations (see Appendix), we have

$$[\breve{\mathbf{Y}}_{u_2}]_{\rm RI} \approx \sum_{u_1=1}^{U_T} \boldsymbol{\Lambda}_{{\rm rx},u_2} \bar{\mathbf{Q}}_{u_2u_1} \boldsymbol{\Lambda}_{{\rm tx},u_1} [\mathbf{C}_{u_1}]_{\rm RI} + [\breve{\boldsymbol{\eta}}_{u_2}]_{\rm RI} \quad (42)$$

where $\boldsymbol{\Lambda}_{{\rm rx},u_2}$ represents the effect of RX IQTM, $\boldsymbol{\Lambda}_{{\rm tx},u_1}$ the effect of TX IQTM, and $\bar{\mathbf{Q}}_{u_2u_1}$ the combined effects of the channel, IQI, CFO, and PN at both TX and RX, as well as SFO and STO. The equation (42) shows the decoupled operations of IQTM and other RF distortions. When $\tau_{{\rm tx},u_1} = \tau_{{\rm rx},u_2} = 0$, the IQTM matrices $\boldsymbol{\Lambda}_{{\rm tx},u_1}$ and $\boldsymbol{\Lambda}_{{\rm rx},u_2}$ reduce to an identity matrix. We will add the OFDM symbol index to the above variables when needed.

III. Impact of IQTM

From (5) or (21), we observe that the effect of IQTM can also be viewed as a specific type of frequency dependent IQI as it takes the same form of the signal model of a frequency-dependent IQ amplitude and phase imbalance as used in the literature (e.g., [4], [16]). But IQTM introduces an additional cascaded frequency-dependent IQI and yields a frequency-dependent IQI characteristic which is significantly different from that of the regular frequency-dependent IQI in the existing literature. To illustrate this, we evaluate the image rejection ratio (IRR) at the RX for three cases: i) system with regular frequency-dependent IQI only (due to $\mu_{R,u_2}(t)$ and

This article has been accepted for publication in a future issue of this journal, but has not been fully edited. Content may change prior to final publication. Citation information: DOI 10.1109/TWC.2017.2696947, IEEE Transactions on Wireless Communications

$$\mathbf{\Lambda}_{\mathrm{rx},u_2} \triangleq \begin{bmatrix} (\Re[\mathbf{\Lambda}_{\mathrm{D}}(\tau_{\mathrm{rx},u_2})] + \Re[\mathbf{\Lambda}_{\mathrm{M}}(\tau_{\mathrm{rx},u_2})]\mathbf{J}), & (\Im[\mathbf{\Lambda}_{\mathrm{M}}(\tau_{\mathrm{rx},u_2})]\mathbf{J} - \Im[\mathbf{\Lambda}_{\mathrm{D}}(\tau_{\mathrm{rx},u_2})]) \\ (\Im[\mathbf{\Lambda}_{\mathrm{D}}(\tau_{\mathrm{rx},u_2})] + \Im[\mathbf{\Lambda}_{\mathrm{M}}(\tau_{\mathrm{rx},u_2})]\mathbf{J}), & (\Re[\mathbf{\Lambda}_{\mathrm{D}}(\tau_{\mathrm{rx},u_2})] - \Re[\mathbf{\Lambda}_{\mathrm{M}}(\tau_{\mathrm{rx},u_2})]\mathbf{J}) \end{bmatrix} \quad (37)$$

$$\mathbf{\Lambda}_{\mathrm{tx},u_1} \triangleq \begin{bmatrix} (\Re[\mathbf{\Lambda}_{\mathrm{D}}(\tau_{\mathrm{tx},u_1})] + \Re[\mathbf{\Lambda}_{\mathrm{M}}(\tau_{\mathrm{tx},u_1})]\mathbf{J}), & (\Im[\mathbf{\Lambda}_{\mathrm{M}}(\tau_{\mathrm{tx},u_1})]\mathbf{J} - \Im[\mathbf{\Lambda}_{\mathrm{D}}(\tau_{\mathrm{tx},u_1})]) \\ (\Im[\mathbf{\Lambda}_{\mathrm{D}}(\tau_{\mathrm{tx},u_1})] + \Im[\mathbf{\Lambda}_{\mathrm{M}}(\tau_{\mathrm{tx},u_1})]\mathbf{J}), & (\Re[\mathbf{\Lambda}_{\mathrm{D}}(\tau_{\mathrm{tx},u_1})] - \Re[\mathbf{\Lambda}_{\mathrm{M}}(\tau_{\mathrm{tx},u_1})]\mathbf{J}) \end{bmatrix} \quad (38)$$

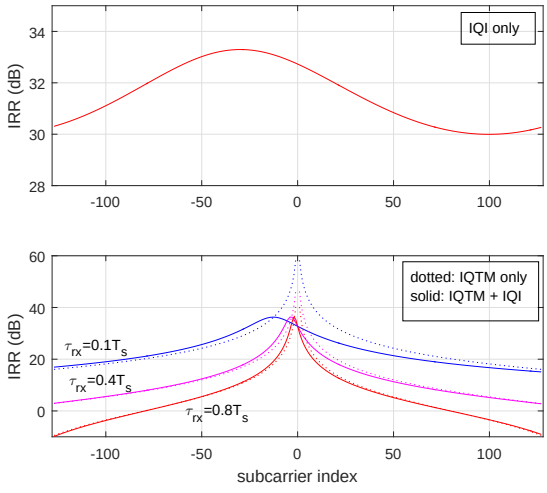

Fig. 3. Impact of IQTM on IRR of an OFDM system with frequency-dependent IQI

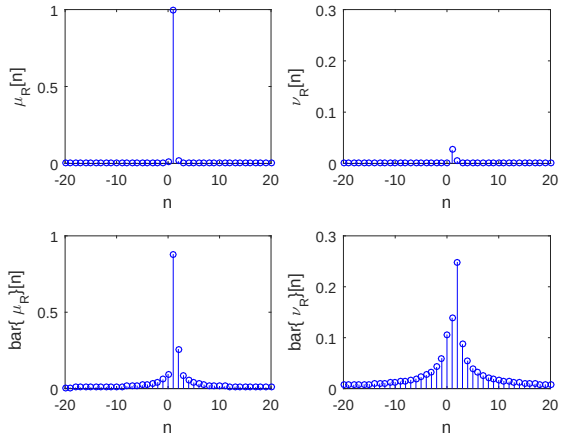

Fig. 4. Equivalent channel length prolonging effect of IQTM (Top: IQI only; Bottom: IQI plus IQTM)

$\nu_{R,u_2}(t)$), ii) system with IQTM τ_{rx,u_2} only, and iii) system with both IQTM and regular frequency-dependent IQI. The IRRs (in dB) at subcarrier n for the three cases are given by

$$\mathrm{IRR}_{\mathrm{IQI}}[n] = 20\log_{10}(|\mathcal{M}_{R,u_2}[n]/\mathcal{N}_{R,u_2}[n]|), \quad (43)$$

$$\mathrm{IRR}_{\mathrm{IQTM}}[n] = 20\log_{10}(\frac{|1+e^{-j2\pi f_n \tau_{\mathrm{rx},u_2}}|}{|1-e^{-j2\pi f_n \tau_{\mathrm{rx},u_2}}|}), \quad (44)$$

$$\mathrm{IRR}_{\mathrm{IQTM+IQI}}[n] = 20\log_{10}(|\bar{\mathcal{M}}_{R,u_2}[n]/\bar{\mathcal{N}}_{R,u_2}[n]|). \quad (45)$$

Let us consider an OFDM system with $N_{\mathrm{DFT}} = 256$, the RX IQTM τ_{rx,u_2}, the RX IQI parameters $a^I_{R,u_2} = 1.02$, $a^Q_{R,u_2} = 0.98$, $\theta^I_{R,u_2} = 1$ degree, $\theta^Q_{R,u_2} = -1$ degree, $p^I_{R,u_2}(t) = 0.01\delta(t) + \delta(t-T_s) + 0.01\delta(t-2T_s)$, and $p^Q_{R,u_2}(t) = 0.01\delta(t) + \delta(t-T_s) + 0.02\delta(t-2T_s)$. Fig. 3 presents the corresponding IRRs of the three cases. We observe that IQTM causes substantial IRR degradation which is more severe at outer subcarriers. For example, at outer subcarriers, IRR is around 30 dB for the system with IQI only but IRR is less than 0 dB for the system with IQI and IQTM $\tau_{\mathrm{rx},u_2} = 0.8T_s$.

Another perspective of the IQTM's effect is that it prolongs the equivalent channel length. For a system with frequency-dependent TX and RX IQI filters of λ taps each and the L-tap channel, the sample-spaced equivalent channel impulse response length (for either the direct channel or the mirror channel) is $L + 2\lambda - 2$ (see eq. (5) and (6) of [16]). Thus, to see the equivalent channel length prolonging effect, we can just observe how IQTM changes the effective IQI filter length. Considering the same system setting as in Fig. 3 with $\tau_{\mathrm{rx},u_2} = 0.4T_s$, we plot in Fig. 4 the effective IQI filter impulse responses for the case with RX IQI only (i.e., $\mu_{R,u_2}[n]$, $\nu_{R,u_2}[n]$) and those for the case with RX IQI and RX IQTM (i.e., $\bar{\mu}_{R,u_2}[n]$, $\bar{\nu}_{R,u_2}[n]$). [1] We observe that IQTM changes the original 3-taps IQI filters into equivalent IQI filters of more than 30 taps. The consequence is that the pilot overhead would substantially increase for each transmission packet since the channels and hence the equivalent channels (incorporating IQI and IQTM) vary over different packets. However, exploiting the specific characteristic (namely IQ mismatch in time delay) of IQTM, we can estimate IQTM separately. The need for IQTM estimation would be infrequent since IQTM does not vary as the channel does. This provides pilot overhead saving, and serves as a motivation for separately addressing IQTM.

IV. IQTM Estimation Metric

In developing the estimator and the pilot design for IQTM, we use the approximate frequency-domain signal model in (42). However, when we evaluate the system performance, the actual signals are generated according to the exact signal model in the time-domain. In this section, we develop pilot-based estimation metric for TX and RX IQTMs. In the metric development, we use pilot preamble(s) where non-zero pilot tones are padded with null pilot tones such that both inter-carrier interference (ICI) and mirror tone interference (MTI) are avoided for non-zero pilot tones and their ICIs

[1] When the equivalent channel impulse response is obtained by IDFT of the frequency domain channel, the negative indexes in the plot correspond to their modulo N_{DFT} but for presentation convenience, we plot them using negative indexes.

This article has been accepted for publication in a future issue of this journal, but has not been fully edited. Content may change prior to final publication. Citation information: DOI 10.1109/TWC.2017.2696947, IEEE Transactions on Wireless Communications

and MTIs are also decoupled. In addition, non-zero pilots of different DAC branches have non-overlapping (decoupled) ICI and MTI spreads. The corresponding pilot designs will be described later. Now, let us consider that DAC branch u_1 transmits a non-zero pilot on subcarrier n and a null pilot on subcarrier $-n$, and observe the received signal (without noise) on subcarrier n and $-n$ at ADC u_2. From Appendix, we know that $\mathbf{A}^{\nu\mu}_{u_2,u_1}[n,n]$ and $\mathbf{A}^{\mu\nu}_{u_2,u_1}[n,n]$ are negligible and $\mathbf{A}^{\mu\mu}_{u_2,u_1}[n,n] \gg \mathbf{A}^{\nu\nu}_{u_2,u_1}[n,n]$. Then, we have

$$\breve{Y}_{u_2}[n] \approx C_{u_1}[n]\mathbf{A}^{\mu\mu}_{u_2,u_1}[n,n], \tag{46}$$

$$\breve{Y}_{u_2}[-n] \approx C^*_{u_1}[n]\left(\mathbf{A}^{\nu\mu}_{u_2,u_1}[-n,n] + \mathbf{A}^{\mu\nu}_{u_2,u_1}[-n,n]\right). \tag{47}$$

Next, define $\xi_n \triangleq \frac{\breve{Y}_{u_2}[-n]}{\breve{Y}^*_{u_2}[n]}$. Then, after some simplification (see Appendix), we obtain ξ_n as in (48) (shown at the top of next page). When there are no IQTMs, i.e., $\tau_{\mathrm{tx},u_1} = \tau_{\mathrm{rx},u_2} = 0$, (48) reduces to

$$\xi_n \approx \frac{\mathcal{N}_{R,u_2}[-n]}{\mathcal{M}^*_{R,u_2}[n]} + \frac{\mathcal{M}_{R,u_2}[-n]D^{\nu}_{u_2,u_1}[-n,-n]}{\mathcal{M}^*_{R,u_2}[n]D^{\mu*}_{u_2,u_1}[n,n]}. \tag{49}$$

We observe that ξ_n without IQTM in (49) varies slowly across n but ξ_n with IQTM in (48) changes faster across n due to the two additional terms caused by IQTMs. The IQTM-induced terms fluctuate more as the IQTM values increase. This implies that the sample variance of ξ_n, denoted σ^2_ξ, is smallest when IQTM reduces to zero. Thus, we use σ^2_ξ as the metric for estimating the IQTMs $(\tau_{\mathrm{tx},u_1}, \tau_{\mathrm{rx},u_2})$. As ξ_n can be viewed as $1/\mathrm{IRR}[n]$, the same conclusion for the metric can also be reached from Fig. 3.

V. Pilot Designs for IQTMs

We can observe from (42) that the RX IQTM can be compensated by multiplying $[\breve{\mathbf{Y}}_{u_2}]_{\mathrm{RI}}$ with the inverse of $\mathbf{\Lambda}_{\mathrm{rx},u_2}$ if τ_{rx,u_2} is known. But we cannot apply a similar compensation approach at the RX for the TX IQTM. Thus, we adopt a novel pilot design approach to handle the TX IQTM. In other words, our approach uses different pilot tones for different TX IQTM estimation candidates but the same pilot tones for all RX IQTM estimation candidates.

A. Joint TX and RX IQTMs or TX-only IQTM

Suppose $\{\tilde{\tau}^{(i)}_{\mathrm{rx},u_2} : i = 1,2,\cdots,n_{\tau,u_2}\}$ and $\{\tilde{\tau}^{(m)}_{\mathrm{tx},u_1} : m = 1,2,\cdots,n_{\tau,u_1}\}$ represent the sets of the trial candidate values for the RX IQTM and the TX IQTM, respectively. Let $\mathbf{C}^{(m)}_{u_1}$ be the $N\times 1$ pilot vector to be used for $\tilde{\tau}^{(m)}_{\mathrm{tx},u_1}$ and its subcarrier indexes are mirror pairs.

First, we define an initial non-zero pilot tone index set $J_{\mathrm{ini}} = \{J^{\mathrm{L}}_{\mathrm{ini}}, J^{\mathrm{R}}_{\mathrm{ini}}\}$ where $J^{\mathrm{L}}_{\mathrm{ini}}$ and $J^{\mathrm{R}}_{\mathrm{ini}}$ represent the index sets of the initial non-zero pilot tones at the left side and the right side of the DC tone, respectively. Suppose that the indexes of the used subcarriers are $-N_L, \cdots, N_R$. To maintain the mirror pair property, $N_L = N_R$. Note that other RF distortions such as PN and IQ amplitude and phase imbalance introduce ICI and MTI in frequency-domain. Assume the one-side significant ICI spread is κ subcarriers and one-side significant MTI spread is ι subcarriers. Recall that our

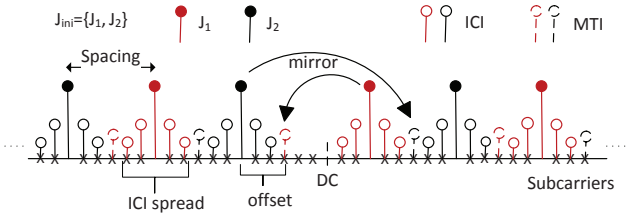

Fig. 5. An illustration of designing J_{ini} for a system with $\kappa = 2$, $\iota = 0$ and two TX IQTM candidates.

estimation metric requires disjointness between ICI spreads at $\{J_{\mathrm{ini}} + k : k = -\kappa,\ldots,\kappa\}$ and MTI at $-J_{\mathrm{ini}}$ (or more conservatively MTI spreads at $\{-J_{\mathrm{ini}}+k : k = -\iota,\ldots,\iota\}$). To achieve this condition, the spacing of non-zero pilot tones must be at least $(2\kappa+2)$ (or more conservatively $(2\kappa+2\iota+2)$) tones at each side of the DC tone, and the non-zero pilot tones at the left side and at the right side are offset by $(\kappa+1)$ (or more conservatively $(\kappa+\iota+1)$) tones. The above spacing guarantees enough spacing for decoupling ICI spreads and MTI (or MTI spread) while the offset ensures that the MTI (or MTI spreads) are disjoint from the ICI spreads. For most practical systems, we observe $\iota = 0$ and hence the two approaches are the same. Below, we present the more conservative design of J_{ini} as

$$J^{\mathrm{R}}_{\mathrm{ini}} = \kappa + 1 : (2\kappa + 2\iota + 2) : N_R, \tag{50}$$

$$J^{\mathrm{L}}_{\mathrm{ini}} = \mathrm{fliplr}(-J^{\mathrm{R}}_{\mathrm{ini}}) - \kappa - \iota - 1 \tag{51}$$

or alternatively as

$$J^{\mathrm{L}}_{\mathrm{ini}} = \mathrm{fliplr}(-\kappa - 1 : (-2\kappa - 2\iota - 2) : -N_L), \tag{52}$$

$$J^{\mathrm{R}}_{\mathrm{ini}} = \mathrm{fliplr}(-J^{\mathrm{L}}_{\mathrm{ini}}) + \kappa + \iota + 1. \tag{53}$$

The reason the starting index in (50) is $\kappa + 1$ or in (52) is $-\kappa - 1$ is to avoid spill-over of ICI spread on the DC tone; otherwise, it may cause problems associated with the DC offset issue[2]. As an example of the design in (50) and (51), consider a system with $N_R = N_L = 86$, $\kappa = 2$ and $\iota = 0$. Then, $J^{\mathrm{R}}_{\mathrm{ini}} = \{3, 9, 15, \ldots, 75, 81\}$ and $J^{\mathrm{L}}_{\mathrm{ini}} = \{-84, -78, -72, \ldots, -12, -6\}$. Fig. 5 also illustrates this example. To see decoupling between ICI spreads and MTI, observe that the ICI spreads of tones at indexes 3 and 9 are at indexes $\{1:5\}$ and $\{7:11\}$ while the MTI of the tone at index -6 appears at index 6. Also note that the ICI spread of tone at index 3 does not cause a DC offset.

We consider a single TX DAC branch first (while keeping DAC branch index u_1 in some variables for a clear connection to the case with multiple DACs), and later we will extend the pilot design to multiple DAC branches. As we will develop different pilot sets for different trial candidate values $\{\tilde{\tau}^{(m)}_{\mathrm{tx},u_1}\}$, let J^{L}_m and J^{R}_m represent the initial non-zero pilot tone index sets at the left and right side of the DC tone for $\tilde{\tau}^{(m)}_{\mathrm{tx},u_1}$. Furthermore, let $[J^{\mathrm{L}}_{\mathrm{ini}}]_k$ and $[J^{\mathrm{R}}_{\mathrm{ini}}]_k$ stand for the kth elements of $J^{\mathrm{L}}_{\mathrm{ini}}$ and $J^{\mathrm{R}}_{\mathrm{ini}}$, respectively. Then, we design the initial pilot

[2]If such issue is insignificant up to ε edge tones of the ICI spread, those starting indexes can begin at $\kappa - \varepsilon + 1$ and $\varepsilon - \kappa - 1$.

This article has been accepted for publication in a future issue of this journal, but has not been fully edited. Content may change prior to final publication. Citation information: DOI 10.1109/TWC.2017.2696947, IEEE Transactions on Wireless Communications

$$\xi_n \approx \frac{\mathcal{N}_{R,u_2}[-n]}{\mathcal{M}^*_{R,u_2}[n]} + \frac{\mathcal{M}_{R,u_2}[-n]D^{\nu}_{u_2,u_1}[-n,-n]}{\mathcal{M}^*_{R,u_2}[n]D^{\mu*}_{u_2,u_1}[n,n]} + \frac{1-e^{j2\pi f_n \tau_{\mathrm{tx},u_1}}}{1+e^{j2\pi f_n \tau_{\mathrm{tx},u_1}}}\Big[\frac{\mathcal{M}_{R,u_2}[-n]D^{\mu}_{u_2,u_1}[-n,-n]}{\mathcal{M}^*_{R,u_2}[n]D^{\mu*}_{u_2,u_1}[n,n]} + \Big(\frac{\mathcal{N}_{R,u_2}[-n]}{\mathcal{M}^*_{R,u_2}[n]}\frac{(1-e^{j2\pi f_n \tau_{\mathrm{rx},u_2}})}{(1+e^{j2\pi f_n \tau_{\mathrm{rx},u_2}})}\Big)\frac{D^{\nu*}_{u_2,u_1}[n,n]}{D^{\mu*}_{u_2,u_1}[n,n]}\Big] + \frac{1-e^{j2\pi f_n \tau_{\mathrm{rx},u_2}}}{1+e^{j2\pi f_n \tau_{\mathrm{rx},u_2}}}. \quad (48)$$

tone index set $J_m = \{J^{\mathrm{L}}_m, J^{\mathrm{R}}_m\}$ for $\tilde{\tau}^{(m)}_{\mathrm{tx},u_1}$ as

$$J^{\mathrm{L}}_m = \{[J^{\mathrm{L}}_{\mathrm{ini}}]_m, [J^{\mathrm{L}}_{\mathrm{ini}}]_{m+n_{\tau,u_1}}, [J^{\mathrm{L}}_{\mathrm{ini}}]_{m+2n_{\tau,u_1}}, \cdots\}, \quad (54)$$

$$J^{\mathrm{R}}_m = \{[J^{\mathrm{R}}_{\mathrm{ini}}]_m, [J^{\mathrm{R}}_{\mathrm{ini}}]_{m+n_{\tau,u_1}}, [J^{\mathrm{R}}_{\mathrm{ini}}]_{m+2n_{\tau,u_1}}, \cdots\}. \quad (55)$$

This allocates J_{ini} among the TX IQTM candidate points in an interleaved frequency division multiplexing manner which provides frequency diversity for each candidate. As an example, consider the system mentioned above with $n_{\tau,u_1} = 2$ candidate points. Then, we have $J^{\mathrm{L}}_1 = \{-84, -72, \ldots, -24, -12\}$, $J^{\mathrm{R}}_1 = \{3, 15, \ldots, 63, 75\}$, $J^{\mathrm{L}}_2 = \{-78, -66, \ldots, -18, -6\}$, and $J^{\mathrm{R}}_2 = \{9, 21, \ldots, 69, 81\}$. Fig. 5 also illustrates J_1 and J_2 for this example.

Next, we design the pilot vector $\mathbf{C}^{(m)}_{u_1}$ for $\tilde{\tau}^{(m)}_{\mathrm{tx},u_1}$. Let $\boldsymbol{p}_m$ denote a $|J_m| \times 1$ vector containing constant amplitude low peak-to-average power ratio (PAPR) sequence for $\tilde{\tau}^{(m)}_{\mathrm{tx},u_1}$, and $\mathbf{\Pi}_m$ represent the $N \times |J_m|$ matrix which assigns $\boldsymbol{p}_m$ to the subcarrier indexes defined by J_m. Let the TX IQTM matrix $\mathbf{\Lambda}_{\mathrm{tx},u_1}$ for $\tau_{\mathrm{tx},u_1} = \tilde{\tau}^{(m)}_{\mathrm{tx},u_1}$ be denoted by $\mathbf{\Lambda}_{\mathrm{tx},u_1}(\tilde{\tau}^{(m)}_{\mathrm{tx},u_1})$. From (42), we observe that we can design $\mathbf{C}^{(m)}_{u_1}$ so that the effect of the TX IQTM for $\tau_{\mathrm{tx},u_1} = \tilde{\tau}^{(m)}_{\mathrm{tx},u_1}$ is pre-compensated. This design is given by

$$[\mathbf{C}^{(m)}_{u_1}]_{\mathrm{RI}} = \mathbf{\Lambda}_{\mathrm{tx},u_1}(-\tilde{\tau}^{(m)}_{\mathrm{tx},u_1})\ [\mathbf{\Pi}_m \boldsymbol{p}_m]_{\mathrm{RI}}. \quad (56)$$

Note that $\mathbf{C}^{(m)}_{u_1}$ has non-zero elements only at the subcarriers defined by J_m for $\tilde{\tau}^{(m)}_{\mathrm{tx},u_1} = 0$ and by $\{\pm J_m\}$ for $\tilde{\tau}^{(m)}_{\mathrm{tx},u_1} \neq 0$. The TX pilot vector is

$$\mathbf{C}_{u_1} = \sum_{m=1}^{n_{\tau,u_1}} \mathbf{C}^{(m)}_{u_1}. \quad (57)$$

The phases of $\{\boldsymbol{p}_m\}$ can be optimized to minimize PAPR of the time-domain signal generated from $\mathbf{C}_{u_1}$. A simpler low-PAPR design is to set $\boldsymbol{p}_m = e^{j\theta_m}\boldsymbol{p}_1$ for $m \neq 1$, and minimize the PAPR over the parameters $\{\theta_m : m = 2, 3, \cdots, n_{\tau,u_1}\}$ and the phases of $\boldsymbol{p}_1$.

If multiple preamble symbols with the symbol index set $\mathcal{T}$ are used, we denote the tone index sets by including the symbol index $t \in \mathcal{T}$. In this case, we have

$$J^{\mathrm{L}}_{\mathrm{ini},t} = J^{\mathrm{L}}_{\mathrm{ini}}, \qquad J^{\mathrm{R}}_{\mathrm{ini},t} = J^{\mathrm{R}}_{\mathrm{ini}},\ t \in \mathcal{T}, \quad (58)$$

$$J^{\mathrm{R}}_{m,t} = \{[J^{\mathrm{R}}_{\mathrm{ini}}]_{\beta_{t,m}+m}, [J^{\mathrm{R}}_{\mathrm{ini}}]_{\beta_{t,m}+m+n_{\tau,u_1}}, [J^{\mathrm{R}}_{\mathrm{ini}}]_{\beta_{t,m}+m+2n_{\tau,u_1}}, \cdots\},\ t \in \mathcal{T}, \quad (59)$$

$$J^{\mathrm{L}}_{m,t} = \{[J^{\mathrm{L}}_{\mathrm{ini}}]_{\beta_{t,m}+m}, [J^{\mathrm{L}}_{\mathrm{ini}}]_{\beta_{t,m}+m+n_{\tau,u_1}}, [J^{\mathrm{L}}_{\mathrm{ini}}]_{\beta_{t,m}+m+2n_{\tau,u_1}}, \cdots\},\ t \in \mathcal{T}, \quad (60)$$

where $\{\beta_{t,m}\}$ are chosen such that non-zero pilot tone indexes of a candidate TX IQTM collected from all the preamble symbols span the subcarriers approximately evenly, and

$$\{J^{\mathrm{R}}_{m_1,t}, J^{\mathrm{L}}_{m_1,t}\} \cap \{J^{\mathrm{R}}_{m_2,t}, J^{\mathrm{L}}_{m_2,t}\} = \emptyset,\ m_1 \neq m_2, t \in \mathcal{T}. \quad (61)$$

Also note that $\{J^{\mathrm{R}}_{m,t_1}, J^{\mathrm{L}}_{m,t_1}\} \cap \{J^{\mathrm{R}}_{m,t_2}, J^{\mathrm{L}}_{m,t_2}\} = \emptyset,\ t_1 \neq t_2$.

For $\tilde{\tau}^{(m)}_{\mathrm{tx},u_1}$ at symbol $t \in \mathcal{T}$, denote the constant amplitude low-PAPR sequence vector by $\boldsymbol{p}_{m,t}$, the subcarrier assignment matrix by $\mathbf{\Pi}_{m,t}$, and the corresponding pilot vector by $\mathbf{C}^{(m)}_{u_1,t}$. Then, $\mathbf{C}^{(m)}_{u_1,t}$ is designed as

$$[\mathbf{C}^{(m)}_{u_1,t}]_{\mathrm{RI}} = \mathbf{\Lambda}_{\mathrm{tx},u_1}(-\tilde{\tau}^{(m)}_{\mathrm{tx},u_1})\ [\mathbf{\Pi}_{m,t}\boldsymbol{p}_{m,t}]_{\mathrm{RI}},\ t \in \mathcal{T}. \quad (62)$$

The TX pilot vector at preamble symbol t is

$$\mathbf{C}_{u_1,t} = \sum_{m=1}^{n_{\tau,u_1}} \mathbf{C}^{(m)}_{u_1,t},\ t \in \mathcal{T}. \quad (63)$$

The same approach of PAPR-minimization can also be done for each preamble symbol by optimizing over the phases of $\{\boldsymbol{p}_{m,t} : m = 1, 2, \cdots, n_{\tau,u_1}\}$ or by setting $\boldsymbol{p}_{m,t} = e^{j\theta_{m,t}}\boldsymbol{p}_{1,t}$ for $m \neq 1$, and optimizing over the parameters $\{\theta_{m,t} : m = 2, 3, \cdots, n_{\tau,u_1}\}$ and the phases of $\boldsymbol{p}_{1,t}$.

B. RX-only IQTM

For the scenario with RX-only IQTM, the pilot design is simply given by the non-zero pilot tone index set J_{ini} as defined in (50) and (51) or (52) and (53), and the constant amplitude low-PAPR sequence transmitted on J_{ini}. All of the RX IQTM estimate candidates use the same received pilots located at $\pm J_{\mathrm{ini}}$. In this case, one preamble symbol is typically sufficient if $|J_{\mathrm{ini}}|$ is reasonably large to yield a reliable sample variance metric σ^2_ξ. If multiple preamble symbols are used, the same preamble can be repeated.

C. Extension to Multiple DACs

For multiple DACs, the above pilot design can be directly generalized while maintaining the property of decoupled ICI and MTI spreads among the non-zero pilot tones. The non-zero pilot tones' indexes are given by (50) and (51) or (53) and (52). These non-zero pilot tones are allocated among different DAC branches in a time-division manner (i.e., using different preamble symbols for different DAC branches) or a distributed frequency-division manner (similar to (55), (54)), or their combination (e.g., time-division for different groups of DACs and frequency division for DACs within each group, or similar to (59), (60)). Then, the non-zero pilot tones of each DAC branch are allocated to different TX IQTM candidate points as in (55) and (54), or (59) and (60). The design principle of the pilot vector for each DAC branch remains the same as that described above.

This article has been accepted for publication in a future issue of this journal, but has not been fully edited. Content may change prior to final publication. Citation information: DOI 10.1109/TWC.2017.2696947, IEEE Transactions on Wireless Communications

VI. Estimation and Compensation of IQTMs

A. Joint estimation of TX and RX IQTMs

Suppose that the system has both TX and RX IQTMs and it uses the corresponding pilots (preambles) described in the previous section. First, we apply compensation of RX IQTM based on a candidate $\tilde{\tau}_{\mathrm{rx},u_2}^{(i)}$ on the received frequency-domain vector at OFDM symbol $t \in \mathcal{T}$ as

$$[\breve{\mathbf{Y}}_{u_2,t}^{(i)}]_{\mathrm{RI}} = \mathbf{\Lambda}_{\mathrm{rx},u_2}(-\tilde{\tau}_{\mathrm{rx},u_2}^{(i)})\ [\breve{\mathbf{Y}}_{u_2,t}]_{\mathrm{RI}} \tag{64}$$

where $\mathbf{\Lambda}_{\mathrm{rx},u_2}(-\tilde{\tau}_{\mathrm{rx},u_2}^{(i)})$ is given by (37) with τ_{rx,u_2} replaced by $-\tilde{\tau}_{\mathrm{rx},u_2}^{(i)}$. Next, for a candidate IQTM pair $(\tilde{\tau}_{\mathrm{tx},u_1}^{(m)}, \tilde{\tau}_{\mathrm{rx},u_2}^{(i)})$ and $n \in J_{m,t}$ with $t \in \mathcal{T}$, we define and compute $\xi_{n,t}^{(m,i)}$ as

$$\xi_{n,t}^{(m,i)} = \frac{\breve{Y}_{u_2,t}^{(i)}[-n]}{(\breve{Y}_{u_2,t}^{(i)}[n])^*} \tag{65}$$

and the estimation metric as a sample variance given by

$$\sigma_\xi^2(\tilde{\tau}_{\mathrm{tx},u_1}^{(m)}, \tilde{\tau}_{\mathrm{rx},u_2}^{(i)}) = \Big(\frac{1}{\sum_{t\in\mathcal{T}}|J_{m,t}|}\sum_{t\in\mathcal{T}}\sum_{n\in J_{m,t}}|\xi_{n,t}^{(m,i)}|^2\Big) - \Big|\frac{1}{\sum_{t\in\mathcal{T}}|J_{m,t}|}\sum_{t\in\mathcal{T}}\sum_{n\in J_{m,t}}\xi_{n,t}^{(m,i)}\Big|^2. \tag{66}$$

Note that different TX IQTM candidate points have different disjoint pilot tones from which their corresponding estimation metric values are computed separately. Among the candidate IQTM pairs $\{(\tilde{\tau}_{\mathrm{tx},u_1}^{(m)}, \tilde{\tau}_{\mathrm{rx},u_2}^{(i)})\}$, the estimator chooses the one which yields the smallest metric value as

$$(\hat{\tau}_{\mathrm{tx},u_1}, \hat{\tau}_{\mathrm{rx},u_2}) = \underset{\{(\tilde{\tau}_{\mathrm{tx},u_1}^{(m)}, \tilde{\tau}_{\mathrm{rx},u_2}^{(i)})\}}{\arg\min}\{\sigma_\xi^2(\tilde{\tau}_{\mathrm{tx},u_1}^{(m)}, \tilde{\tau}_{\mathrm{rx},u_2}^{(i)})\}. \tag{67}$$

B. Estimation of TX-only IQTM

Let us consider the scenario with TX-only IQTM and the corresponding pilots as described in the previous section. Then, no RX side compensation is needed and we define and compute

$$\xi_{n,t}^{(m)} = \frac{\breve{Y}_{u_2,t}[-n]}{(\breve{Y}_{u_2,t}[n])^*}, \quad n \in J_{m,t},\ t \in \mathcal{T}, \tag{68}$$

$$\sigma_\xi^2(\tilde{\tau}_{\mathrm{tx},u_1}^{(m)}) = \Big(\frac{1}{\sum_{t\in\mathcal{T}}|J_{m,t}|}\sum_{t\in\mathcal{T}}\sum_{n\in J_{m,t}}|\xi_{n,t}^{(m)}|^2\Big) - \Big|\frac{1}{\sum_{t\in\mathcal{T}}|J_{m,t}|}\sum_{t\in\mathcal{T}}\sum_{n\in J_{m,t}}\xi_{n,t}^{(m)}\Big|^2. \tag{69}$$

Then, the corresponding TX IQTM estimator is given by

$$\hat{\tau}_{\mathrm{tx},u_1} = \arg_{\{\tilde{\tau}_{\mathrm{tx},u_1}^{(m)}\}}\min\{\sigma_\xi^2(\tilde{\tau}_{\mathrm{tx},u_1}^{(m)})\}. \tag{70}$$

C. Estimation of RX-only IQTM

Suppose that IQTM only exists at the RX and the corresponding pilots described in the previous section are used. First, we apply compensation of RX IQTM based on a candidate $\tilde{\tau}_{\mathrm{rx},u_2}^{(i)}$ as in (64) to the frequency-domain received vector at preamble symbol $t \in \mathcal{T}$. Then, we define and compute

$$\xi_{n,t}^{(i)} = \frac{\breve{Y}_{u_2,t}^{(i)}[-n]}{(\breve{Y}_{u_2,t}^{(i)}[n])^*}, \quad n \in J_{\mathrm{ini}},\ t \in \mathcal{T}, \tag{71}$$

$$\sigma_\xi^2(\tilde{\tau}_{\mathrm{rx},u_2}^{(i)}) = \Big(\frac{1}{|\mathcal{T}||J_{\mathrm{ini}}|}\sum_{t\in\mathcal{T}}\sum_{n\in J_{\mathrm{ini}}}|\xi_{n,t}^{(i)}|^2\Big) - \Big|\frac{1}{|\mathcal{T}||J_{\mathrm{ini}}|}\sum_{t\in\mathcal{T}}\sum_{n\in J_{\mathrm{ini}}}\xi_{n,t}^{(i)}\Big|^2. \tag{72}$$

The corresponding RX IQTM estimator is given by

$$\hat{\tau}_{\mathrm{rx},u_2} = \arg_{\{\tilde{\tau}_{\mathrm{rx},u_2}^{(i)}\}}\min\{\sigma_\xi^2(\tilde{\tau}_{\mathrm{rx},u_2}^{(i)})\}. \tag{73}$$

D. IQTM Estimation in MIMO System

In a MIMO system with U_T DAC branches and U_R ADC branches, we can further improve the estimation performance by averaging across relevant MIMO branches. Recall that the pilot tones of U_T TX DAC branches are disjoint in frequency and/or time. These U_T disjoint pilot sets experience the same RX IQTM at an ADC branch. Thus, at the output of ADC branch u_2, our estimator based on U_T pilot sets gives U_T estimates of the same RX IQTM for the ADC branch u_2. We propose to average these U_T estimates to enhance the RX IQTM estimation performance. As an example of averaging, we use the majority rule to select the final estimate. In a similar manner, TX IQTM of a DAC branch is estimated at the output of each of the U_R ADC branches and these U_R estimates of TX IQTM of that DAC branch can be averaged to improve the TX IQTM estimation performance.

Next, we analytically assess the performance of the majority rule MIMO averaging. Our investigation results (as will be presented later) show that random normalized IQTMs (i.e., $\tau_{\mathrm{tx},u_1}/T_s$ and $\tau_{\mathrm{rx},u_1}/T_s'$) which are uniformly distributed within the range $[-1/8, 1/8]$ give almost the same bit error rate (BER) performance as the system with no IQTMs. Thus, we consider discretized IQTM values with a normalized resolution of 1/4, which allows us to evaluate estimation success or failure probabilities. We also observe in our investigation (as will be shown later) that the proposed estimator before MIMO averaging gives the correct estimate most of the times and almost all of the errors correspond to one or two adjacent candidate points at each side of the actual IQTM point. Thus, it is sufficient to consider a total of 5 possible points for the estimate, and denote their probabilities by P_i, $i = 0, 1, \cdots, 4$ where P_0 represents the probability of correct estimation. As the estimates in the above averaging are independent, after combining U estimates by the majority rule, the estimation success probability is given by

$$P_{\mathrm{success}} = \sum_{k=\lceil U/5\rceil}^{U} P_0^k Q(U-k,k) + \sum_{k=\lceil U/5\rceil}^{U}\sum_{m=1}^{\lfloor (U-k)/k\rfloor}\frac{1}{m}P_0^k Q'(U-k,k,m) \tag{74}$$

This article has been accepted for publication in a future issue of this journal, but has not been fully edited. Content may change prior to final publication. Citation information: DOI 10.1109/TWC.2017.2696947, IEEE Transactions on Wireless Communications

where $\lfloor X \rfloor$ ($\lceil X \rceil$) is the floor (ceiling) operation which rounds X to the nearest integer less (greater) than or equal to X and $Q(X,Y) = \sum \binom{X}{k_1}\binom{X-k_1}{k_2}\binom{X-k_1-k_2}{k_3} P_1^{k_1} P_2^{k_2} P_3^{k_3} P_4^{k_4}$ with the constraint that k_1, k_2, k_3, k_4 are non-negative integers, $k_1 + k_2 + k_3 + k_4 = X$ and $\max(k_1, k_2, k_3, k_4) < Y$. Next, $Q'(X, Y, m) = \sum \binom{X}{k_1}\binom{X-k_1}{k_2}\binom{X-k_1-k_2}{k_3} P_1^{k_1} P_2^{k_2} P_3^{k_3} P_4^{k_4}$ with the constraint $k_1 + k_2 + k_3 + k_4 = X$, $\max(k_1, k_2, k_3, k_4) = Y$ and m variables from k_1, k_2, k_3, k_4 have the same maximum value Y. If there is no such k_1, k_2, k_3, k_4 which satisfy the constraint, $Q(X,Y)$ or $Q'(X,Y,m)$ equals to 0. In (74), the first term corresponds to the case where the correct candidate point has more counts than any other candidate. The second term is due to the tied case where the correct candidate point and one or more other candidate points have the same majority count.

E. Protocol for IQTM Compensation

As the characteristics of the TX and RX circuit paths can be different, the TX and RX IQTMs for uplink and downlink can be different. Thus, in practice, pilot transmission and estimation of TX and RX IQTMs should be done for both uplink and downlink. The RX IQTM can be compensated at the RX. However, the TX IQTM cannot be compensated at the RX and hence it should be fed back to the TX and compensation should be done at the TX. Thus, for IQTM estimation/compensation for both uplink and downlink, we propose the transmission protocol given in Fig. 6. Note that majority rule MIMO averaging is applied in step 2 and item i of step 4 in the protocol. In step 3, pilots and data tones (feedback information) of different UEs are disjoint in the time domain (TDM), frequency domain (FDM) or a combination of both (TDM+FDM). In items ii and iii of step 4, averaging across UEs is performed, for example, by majority rule in the same way as in MIMO averaging. Other parts of the protocol steps are self-explanatory from the description, thus further elaboration is omitted.

We note that the UE averaging is essentially the same as additional MIMO averaging, thus its performance can be obtained from (74) where $\{P_i\}$ now represent probabilities of the estimates after MIMO averaging at a UE but before the UE averaging.

As IQTMs typically do not change even over a long time interval, it is not necessary to frequently transmit pilots and estimate IQTM. Each transceiver just stores its TX and RX IQTM estimate values and applies the corresponding compensation at the RX or at the TX. If desired, regular fine tuning of the IQTM estimate values can be done by the same approach and by appropriately averaging the estimate values.

F. IQTM Compensation

For a transceiver with stored IQTM estimates of $\{\hat{\tau}_{\mathrm{tx},u_1}\}$ and $\{\hat{\tau}_{\mathrm{rx},u_2}\}$, the TX IQTM compensation is performed on the frequency-domain data vector as

$$[\tilde{\mathbf{C}}_{u_1}]_{\mathrm{RI}} = \mathbf{\Lambda}_{\mathrm{tx},u_1}(-\hat{\tau}_{\mathrm{tx},u_1})\ [\mathbf{C}_{u_1}]_{\mathrm{RI}} \tag{75}$$

where $\tilde{\mathbf{C}}_{u_1}$ becomes IDFT inputs for OFDM signal generation. The RX IQTM compensation is performed on the DFT output

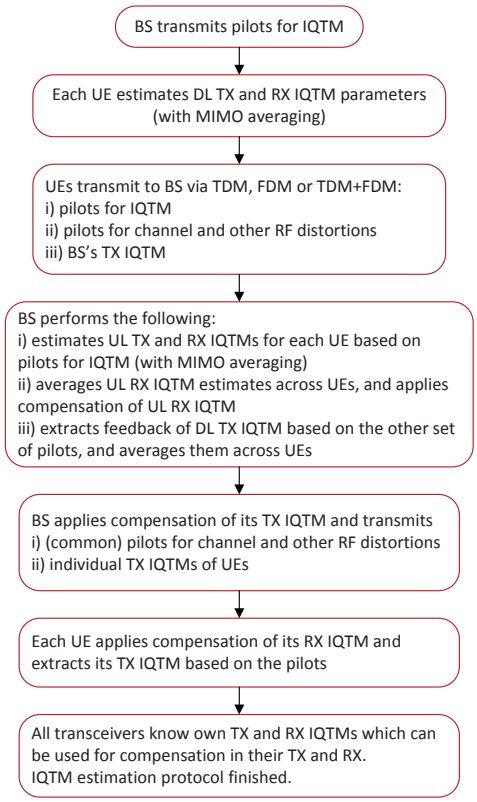

Fig. 6. Protocol sequence for TX and RX IQTM estimation/compensation for uplink and downlink. (TDM=time-division multiplexing, FDM=frequency-division multiplexing)

frequency-domain vector at RX as

$$[\tilde{\mathbf{Y}}_{u_2}]_{\mathrm{RI}} = \mathbf{\Lambda}_{\mathrm{rx},u_2}(-\hat{\tau}_{\mathrm{rx},u_2})\ [\breve{\mathbf{Y}}_{u_2}]_{\mathrm{RI}} \tag{76}$$

where $\tilde{\mathbf{Y}}_{u_2}$ is input to the modulation slicer or data detector. In the above, we presented baseband DSP-based compensation for IQTM. If the transceiver has multi-phase filters or DAC/ADC with adjustable sampling instants for introducing different delays at the TX and RX chains, IQTM compensation can also be implemented by such hardware-based mechanism.

VII. Performance Evaluation

A. System Setting

We consider an OFDM system with 64 antennas at BS and 4 antennas at UE. The subcarrier spacing is 1.44 MHz and the carrier frequency is 73 GHz. We use two settings for bandwidth, namely, 250 MHz and 2 GHz, the corresponding DFT sizes are 256 and 2048, and the number of used subcarriers is 173 and 1388, respectively. The channel model is based on the 3GPP LTE channel model [29] with two clusters where each cluster has 20 sub-paths, the second clusters delay is about 80 ns (based on Huawei's mm-wave channel measurements) and its power is -9 dB with reference to the first cluster. Analog beamforming is applied based on the mean arrival angle of the sub-paths of the first cluster. We consider a single data stream with 16-QAM. The PN power spectral densities (PSD) at TX and RX are independently modeled as $\mathrm{PSD}(f) = \mathrm{PSD}(0)[1 + (\frac{f}{f_z})^2]/[1 + (\frac{f}{f_p})^2]$ where PSD(0) = -60 dBc/Hz, PSD(100k)

This article has been accepted for publication in a future issue of this journal, but has not been fully edited. Content may change prior to final publication. Citation information: DOI 10.1109/TWC.2017.2696947, IEEE Transactions on Wireless Communications

= -75 dBc/Hz and PSD(∞) = -130 dBc/Hz. The CFOs at TX and RX sides are independent and uniformly distributed within the range of ± 1 ppm, the RX SFO is set at 1 ppm and the RX STO is uniformly distributed within $[-T_s'/2, T_s'/2]$. Frequency-independent IQIs are independent at TX and RX sides and they are modeled with uniform distributions with the range $[-4, 4]$ for $20\log_{10}[a^I/a^Q]$, and the range $[-5, 5]$ degrees for $\theta^I - \theta_Q$. Frequency-dependent IQI filters are set as $p^I_{R,u_2}(t) = 0.01\delta(t) + \delta(t - T_s) + 0.01\delta(t - 2T_s)$, and $p^Q_{R,u_2}(t) = 0.01\delta(t) + \delta(t - T_s') + 0.02\delta(t - 2T_s')$. The mobile speed is 10 km/h. We assume no nonlinear distortion. We use $\kappa = 2$ and $\iota = 0$ and they are set according to [17]. In the simulation, signals are generated in the time domain with 4 times oversampling of the DFT sampling frequency.

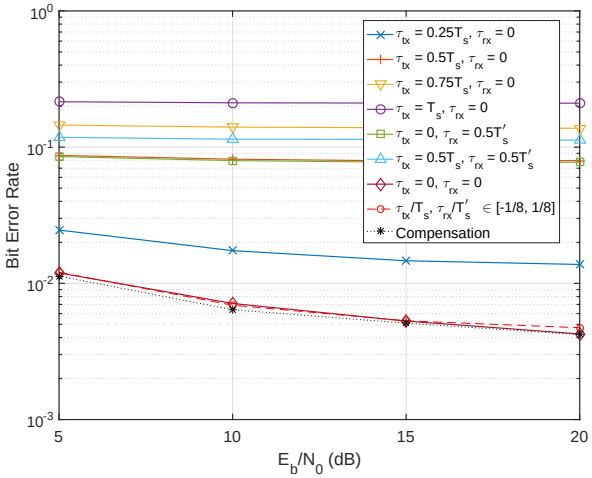

Fig. 7. The impacts of IQTMs on the system's BER performance.

B. Impact of IQTM on BER

We first evaluate the impact of IQTM on system's BER, thus no IQTM compensation is applied here. We consider the system with 250 MHz bandwidth where an OFDM preamble symbol is followed by a pilot-data multiplexed OFDM symbol carrying 16-QAM symbols and pilot tones. Here, we assume frequency-independent IQI[3]. The preamble and pilots are for estimating the channel and RF distortions (other than IQTM). These preamble and pilot designs, their corresponding estimators and data detection are according to [17]. In Fig. 7, we present the effects of IQTMs on BER for different E_b/N_0 values. We evaluate BER for systems with TX-only IQTM, RX-only IQTM, and both TX and RX IQTMs. We observe that the BER performance degrades as the IQTM increases and the BER performances for TX-only IQTM and RX-only IQTM are practically the same. The IQTMs at both TX and RX cause more BER degradation than the IQTM at one side only. We also include a random (uniform) IQTMs with the normalized range of $[-1/8, 1/8]$, and its BER performance is almost the same as that of the system with no IQTMs. This provides a guideline for setting the spacing of the candidate normalized IQTM values to be $1/4$ for the considered system. Furthermore, it also allows us to discretize the actual IQTM values with the spacing of $1/4$ (which we use in our later investigations) which in turn enables us to assess the estimation failure probabilities of our IQTM estimators. Next, we observe that the IQTM-induced BER degradation is substantial if the normalized IQTMs are larger than 1/8 and no IQTM compensation is applied. The above BER results clearly demonstrate that IQTM estimation and compensation schemes are needed to counter the effects of IQTM.

To illustrate the performance of the proposed IQTM compensation, we also include in Fig. 7 the BER performance (denoted "Compensation") obtained after our proposed IQTM compensation for the case with $\tau_{\rm tx} = 0.5T_s$ and $\tau_{\rm rx} = 0.5T_s'$. The proposed approach achieves the same BER performance as the case without IQTMs, thus illustrating its effectiveness.

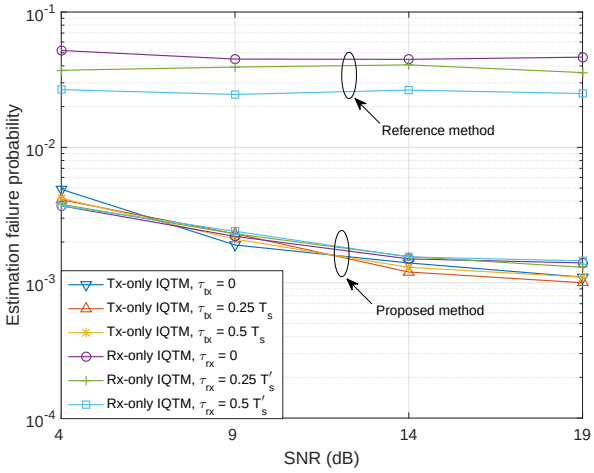

Fig. 8. Estimation failure probabilities for systems with TX-only IQTM and RX-only IQTM

C. Estimator Performance

The estimator in [27] assumes that CFO is pre-compensated and other RF distortions are ignored. Its estimator uses two preambles with frequency-domain symbols $\{C_1[k]\}$ and $\{C_2[k]\}$ separately and requires that $\frac{C_1^*[N-k+1]}{C_1[k]} - \frac{C_2^*[N-k+1]}{C_2[k]} \neq 0$ for $k \in \mathcal{P}$ where $\mathcal{P}$ is the pilot index set. The signal is intentionally transmitted on pairs of mirror subcarriers to enable the key metric function $D[k] = \frac{\breve{Y}_2[k] - C_2[k]\hat{H}[k]}{\breve{Y}_2^*[N-k+1] - C_{\rm ideal}[k]\hat{H}[N-k+1]}$ in the RX-only IQTM case, where $C_{\rm ideal}[k] = C_2[k]C_1^*[N-k+1]/C_1[k]$ and $\hat{H}[k] = \breve{Y}_1[k]/C_1[k]$. Reference [27] estimates $\tau_{\rm rx}$ by comparing the variance of $\{D[k], k \in \mathcal{P}\}$ to heuristic thresholds.

We first evaluate the TX-only and RX-only IQTM cases for the system with 250 MHz bandwidth and frequency-independent IQI. For the RX-only IQTM case, we use one preamble symbol with non-zero pilot tone spacing of 6 tones at each side of the DC tone and use the candidate set $\{\tilde{\tau}_{\rm rx}^{(i)}\}$

[3]Pilot designs and data detection scheme for the considered system with frequency-dependent IQI are not available in the literature and developing them constitutes another research problem which is outside the scope of this paper.

This article has been accepted for publication in a future issue of this journal, but has not been fully edited. Content may change prior to final publication. Citation information: DOI 10.1109/TWC.2017.2696947, IEEE Transactions on Wireless Communications

$= \{-T_s', -0.75T_s', \cdots, T_s'\}$. The reference estimator uses two preamble symbols and each symbol uses the same amount of pilots and the same pilot tone spacing as the proposed estimator. For the TX-only IQTM case, we use the candidate set $\{\tilde{\tau}_{\text{tx}}^{(i)}\} = \{-T_s, -0.75T_s, \cdots, T_s\}$. The number of preamble symbols is the same as the number of TX IQTM candidate points. Each preamble symbol has non-zero pilot tones with tone spacing of 6 tones at each side of the DC tone and these non-zero pilot tones are assigned alternately among the IQTM candidate points as described in Section V.

Fig. 8 presents the estimation failure probability of the reference estimator in [27] for the RX-only IQTM case and the proposed IQTM estimators for the TX-only and RX-only IQTM cases. We see that the proposed RX IQTM estimator has significant advantage compared to the reference estimator. Note that the reference estimator is developed without considering TX IQTM, so it cannot estimate the TX IQTM. We also observe that the estimation failure probabilities of the proposed estimators for the TX-only and RX-only IQTM cases are similar.

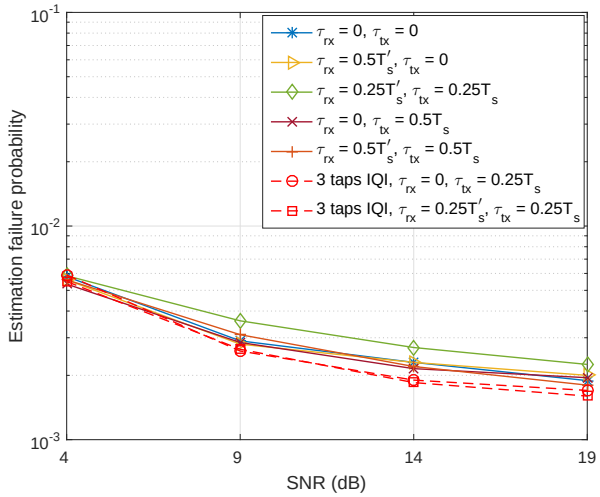

Fig. 9. TX IQTM estimation failure probability of the proposed method in systems with both TX and RX IQTMs

Next, we evaluate the estimator performance in systems with both TX and RX IQTMs for both cases of frequency-independent IQI and frequency-dependent IQI (3 taps). For the proposed estimator, we use the candidate set $\{\tilde{\tau}_{\text{tx}}^{(i)}\} = \{-T_s, -0.75T_s, \cdots, T_s\}$ and $\{\tilde{\tau}_{\text{rx}}^{(i)}\} = \{-T_s', -0.75T_s', \cdots, T_s'\}$. Fig. 9 and Fig. 10 show the estimation failure probabilities of the TX IQTM and the RX IQTM, respectively, for the proposed method under several IQTM settings. In Fig. 10, we also include the performance of the reference estimator when $\tau_{\text{tx}} = 0.25T_s$. We observe that the reference estimator fails in the presence of TX IQTM. The reference estimator relies on heuristic thresholds which are calculated based on RX-only IQTM candidates. In the presence of TX IQTM, the metric used in [27] is no longer valid and those heuristic thresholds are not applicable any more. Comparing with Fig. 8, IQTMs at both the TX and RX cause larger estimation failure probability than individual IQTM cases.

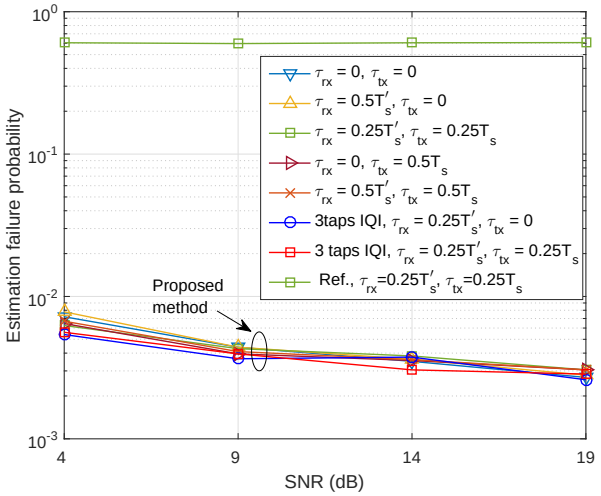

Fig. 10. RX IQTM estimation failure probability of the proposed method in systems with both TX and RX IQTMs

But the proposed method still gives good performance. The estimation failure probabilities of different τ_{tx} and τ_{rx} values are similar.

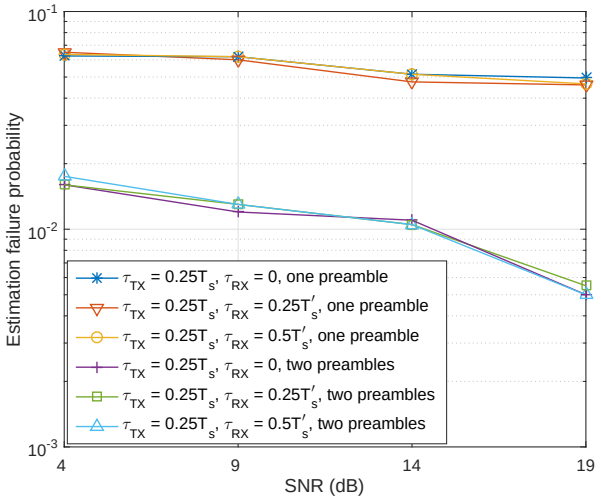

Fig. 11. TX IQTM estimation failure probability for systems with both TX and RX IQTMs (2 GHz bandwidth)

Fig. 11 and Fig. 12 present the TX and RX IQTM estimation performance of the proposed method in the system with 2 GHz bandwidth in the presence of both the TX and RX IQTMs. We use $\{\tilde{\tau}_{\text{rx}}^{(i)}\} = \{-T_s', -0.75T_s', \cdots, T_s'\}$ and $\{\tilde{\tau}_{\text{tx}}^{(i)}\} = \{-0.5T_s, -0.25T_s, \cdots, 0.5T_s\}$. Here, we test with one or two preamble symbols only. We observe that using two preamble symbols gives a reasonably good estimation failure rate of about 1% for both TX and RX IQTMs.

Next, to illustrate performance improvement of MIMO averaging, we consider a MIMO system with $U_T = U_R = 4$ as an example. Suppose that the error probability mass function before MIMO averaging is given by $[P_0, P_1, P_2, P_3, P_4]$ which correspond to probabilities of selecting 5 candi-

This article has been accepted for publication in a future issue of this journal, but has not been fully edited. Content may change prior to final publication. Citation information: DOI 10.1109/TWC.2017.2696947, IEEE Transactions on Wireless Communications

$$P_{\text{success}} = P_0^4 + \binom{4}{1} P_0^3(1-P_0) + 3!P_0(P_1P_2P_3 + P_1P_2P_4 + P_1P_3P_4 + P_2P_3P_4) + \binom{4}{2} P_0^2\left[2(P_1P_2 + P_1P_3 + P_1P_4 + P_2P_3 + P_2P_4 + P_3P_4) + \frac{1}{2}\sum_{i=1}^{4} P_i^2\right]. \quad (77)$$

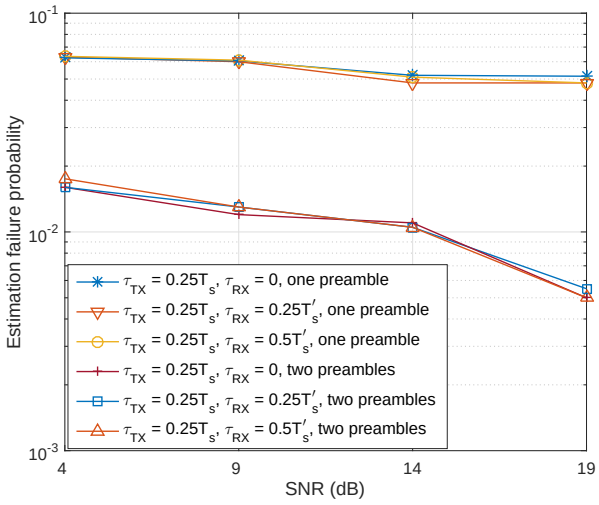

Fig. 12. RX IQTM estimation failure probability for systems with both TX and RX IQTMs (2 GHz bandwidth)

date IQTM values with the normalized estimation error $[0, -0.25, 0.25, -0.5, 0.5]$, respectively. From (74), the estimation success probability after the majority rule MIMO averaging can be obtained as in (77). Taking the results in Fig 9 as an example, the estimation failure probability of a certain DAC branch TX IQTM is about 5.6×10^{-3} at 4dB SNR for each single estimator (before MIMO averaging). The corresponding probabilities obtained by simulation are given by $P_0 = 0.9944$, $P_1 \approx P_2 = 0.0024$, and $P_3 \approx P_4 = 0.0004$. Substituting these values into (77) gives the estimation failure probability of the MIMO averaging as 3.579×10^{-5} and the simulation gives a matched result of 3.6×10^{-5}. Similarly, in Fig 10, the estimation failure probability of a certain ADC branch RX IQTM is about 6.1×10^{-3} at 4dB SNR for each single estimator (before MIMO averaging). The corresponding probabilities obtained by simulation are given by $P_0 = 0.9939$, $P_1 \approx P_2 = 0.0026$, and $P_3 \approx P_4 = 0.0004$. With these values, (77) gives the estimation failure probability of the MIMO averaging as 4.188×10^{-5} and the simulation gives a matched result 4.165×10^{-5}. Thus, we observe that the estimator performance can be significantly improved by means of MIMO averaging. As UE averaging plays the same role, its additional performance improvement can also be directly understood.

D. Pilot Overhead and Estimator Complexity

As IQTMs typically do not change much, their estimation need not be performed frequently. The pilot overhead depends on the number of TX IQTM candidate points, the phase noise one-side ICI spread (as it determines the non-zero pilot tone spacing), and the number of used subcarriers (as the ICI level on a subcarrier depends on it). For example, for $\tau_{\text{tx},u_1}/T_s \in [-0.5, 0.5]$ with 5 TX IQTM candidate points and 250 MHz bandwidth, we can use 5 pilot symbols instead of 9 symbols and obtain similar estimation performance (the plots of which are omitted due to space limitation). For reliable IQTM estimation in the systems with the phase noise one-side ICI spread of two subcarriers, and the subcarrier spacing of 1.44 MHz, the pilot overhead we use is one OFDM symbol of duration $0.844\mu s$ (about 28 non-zero pilot tones) per TX IQTM candidate point for 250 MHz bandwidth (173 used subcarriers) and two OFDM symbols (with OFDM symbol duration of $0.787\mu s$) per 5 TX IQTM candidate points (about 92 non-zero pilot tones per TX IQTM candidate point) for 2 GHz bandwidth (1388 used subcarriers). The pilot overhead could be less for milder phase noises.

Next, we provide the computational complexity of the joint TX and RX IQTM estimator after the RX DFT operation. Suppose for n_{τ,u_1} TX IQTM candidate points, n_{τ,u_2} RX IQTM candidate points, and U_T TX DAC branches, there are M OFDM symbols, each with K non-zero pilot tones. Then, from (64), (65), (66), and (67), the estimator requires $n_{\tau,u2}[8KM + (2KM + n_{\tau,u_1})U_T]$ real multiplications or divisions, $n_{\tau,u2}[5KM + (4KM - n_{\tau,u_1})U_T]$ real additions or subtractions, and $U_T(n_{\tau,u_1}n_{\tau,u_2} - 1)$ real comparisons. For example, for the considered system with $N_{\text{DFT}} = 256$, $U_T = 1$, $\tau_{\text{tx},u_1} \in [-0.5T_s, 0.5T_s]$, and $\tau_{\text{rx},u_2} \in [-0.5T'_s, 0.5T'_s]$, we can use $K = 28$, $n_{\tau,u_1} = 5$, $n_{\tau,u_2} = 5$, $M = 5$ and the estimator requires 7,025 real multiplications, 6,275 real additions, and 24 real comparisons.

VIII. Conclusions

We have studied the effects of IQTMs on mm-wave OFDM systems with RF distortions and developed corresponding signal model, novel pilot designs, IQTM estimators, and corresponding protocols for IQTM compensation. Our investigation results are summarized below. IQTMs cause a cascaded IQI scenario with substantially different characteristics from the regular (commonly considered) IQI. These IQTMs can prolong the effective channel length and significantly degrade the IRR (more pronounced at outer subcarriers) and the BER performance. An IQTM value larger than $1/8$ of the normal sampling period causes substantial BER degradation to the considered system and the larger the IQTM value, the worse the BER is. Our estimators apply RX-side IQTM compensation for each RX IQTM candidate and a disjoint set of specifically designed pilot tones for each TX IQTM candidate. Resolution of IQTM candidate points should be at least 4 points per the normal sampling period. Our estimation metric exploits the

This article has been accepted for publication in a future issue of this journal, but has not been fully edited. Content may change prior to final publication. Citation information: DOI 10.1109/TWC.2017.2696947, IEEE Transactions on Wireless Communications

fact that a larger IQTM causes more fluctuation of IRR across subcarriers and it proves to be an effective metric. The proposed IQTM estimators and compensators can be implemented without requiring compensation of other RF distortions. The simulation results show that the proposed pilot designs and IQTM estimators substantially outperform the existing method in terms of estimation performance and general applicability. Furthermore, the proposed MIMO averaging and UE averaging substantially enhance IQTM estimation performance. Overall, IQTM is an important issue for mm-wave systems and the proposed approach offers an effective solution.

APPENDIX

This appendix presents detailed steps in developing the frequency domain signal models. First, substituting $\mathcal{F}\{\text{Eq. (18)}\}$ into $\mathcal{F}\{\text{Eq. (22)}\}$ gives

$$\begin{aligned}\breve{Y}_{u_2}(f) = \bar{\mathcal{M}}_{R,u_2}(f)\{R_{u_2}(f) * \Psi_{R,u_2}(f+\alpha_{u_2})\}G_R(f) \\ + \bar{\mathcal{N}}_{R,u_2}(f)\{R^*_{u_2}(-f) * \Psi^*_{R,u_2}(-f+\alpha_{u_2})\}G^*_R(-f).\end{aligned} \tag{78}$$

Next, substituting $\mathcal{F}\{\text{Eq. (14)}\}$ into $\mathcal{F}\{\text{Eq. (15)}\}$ gives

$$\begin{aligned}R_{u_2}(f) = \sum_{v_2=1}^{V_R}\Big\{\sum_{u_1=1}^{U_T}\sum_{v_1=1}^{V_T} e^{j\theta_{T,u_1,v_1}} X_{u_1,v_1}(f) H^{u_2,v_2}_{u_1,v_1}(f) \\ + W_{u_2,v_2}(f)\Big\} e^{j\theta_{R,u_2,v_2}}.\end{aligned} \tag{79}$$

Similarly, substitute (2) into $\mathcal{F}\{\text{Eq. (11)}\}$ and then into (79), (78), and (25), successively. Then, some lengthy but straightforward manipulation gives (27) with its variables defined in (80)-(84) (shown at the top of next page).

Next, the Fourier transforms of (12), (13), (23), and (24) give

$$\begin{aligned}\bar{\mathcal{M}}_{T,u_1,v_1}(f) =& \mathcal{M}_{T,u_1,v_1}(f)\frac{1+e^{-j2\pi f\tau_{\text{tx},u_1}}}{2} \\ &+ \mathcal{N}_{T,u_1,v_1}(f)\frac{1-e^{-j2\pi f\tau_{\text{tx},u_1}}}{2},\end{aligned} \tag{85}$$

$$\begin{aligned}\bar{\mathcal{N}}_{T,u_1,v_1}(f) =& \mathcal{M}_{T,u_1,v_1}(f)\frac{1-e^{-j2\pi f\tau_{\text{tx},u_1}}}{2} \\ &+ \mathcal{N}_{T,u_1,v_1}(f)\frac{1+e^{-j2\pi f\tau_{\text{tx},u_1}}}{2},\end{aligned} \tag{86}$$

$$\begin{aligned}\bar{\mathcal{M}}_{R,u_2}(f) =& \mathcal{M}_{R,u_2}(f)\frac{1+e^{-j2\pi f\tau_{\text{rx},u_2}}}{2} \\ &+ \mathcal{N}^*_{R,u_2}(-f)\frac{1-e^{-j2\pi f\tau_{\text{rx},u_2}}}{2},\end{aligned} \tag{87}$$

$$\begin{aligned}\bar{\mathcal{N}}_{R,u_2}(f) =& \mathcal{M}^*_{R,u_2}(-f)\frac{1-e^{-j2\pi f\tau_{\text{rx},u_2}}}{2} \\ &+ \mathcal{N}_{R,u_2}(f)\frac{1+e^{-j2\pi f\tau_{\text{rx},u_2}}}{2}.\end{aligned} \tag{88}$$

We observe that $\bar{\mathcal{M}}_{T,u_1,v_1}(f)$, $\bar{\mathcal{N}}_{T,u_1,v_1}(f)$, $\bar{\mathcal{M}}_{R,u_2}(f)$, and $\bar{\mathcal{N}}_{R,u_2}(f)$ do not change much within a subcarrier bandwidth (or within the main bandwidth of $\gamma_T(f)$ and $\gamma_R(f)$) since the underlying frequency-dependent IQI filter frequency responses do not vary much within a subcarrier bandwidth. Using this fact in (80), we obtain (89) and (90) shown at the next page and (91)-(92) shown below:

$$D^{\mu}_{u_2,u_1}[n,l] \triangleq \sum_{v_1=1}^{V_T} \mathcal{M}_{T,u_1,v_1}[l] e^{j\theta_{T,u_1,v_1}} D_{u_2,u_1,v_1}[n,l] \tag{91}$$

$$D^{\nu}_{u_2,u_1}[n,l] \triangleq \sum_{v_1=1}^{V_T} \mathcal{N}_{T,u_1,v_1}[l] e^{j\theta_{T,u_1,v_1}} D_{u_2,u_1,v_1}[n,l] \tag{92}$$

Similarly, we obtain (93)-(95) shown at the next page. For the used subcarriers, we can express (89), (93), (94), and (95) in the matrix form as

$$\mathbf{A}^{\mu\mu}_{u_2,u_1} \approx \mathbf{\Lambda}_{\bar{\mathcal{M}}_{R,u_2}}\left(\mathbf{D}^{\mu}_{u_2,u_1}\mathbf{\Lambda}_{\text{D}}(\tau_{\text{tx},u_1}) + \mathbf{D}^{\nu}_{u_2,u_1}\mathbf{\Lambda}_{\text{M}}(\tau_{\text{tx},u_1})\right), \tag{96}$$

$$\begin{aligned}\mathbf{A}^{\nu\nu}_{u_2,u_1} \approx& \mathbf{\Lambda}_{\bar{\mathcal{N}}_{R,u_2}}\Big(\mathbf{J}\mathbf{D}^{\mu*}_{u_2,u_1}\mathbf{\Lambda}^*_{\text{M}}(\tau_{\text{tx},u_1})\mathbf{J} \\ &+ \mathbf{J}\mathbf{D}^{\nu*}_{u_2,u_1}\mathbf{\Lambda}^*_{\text{D}}(\tau_{\text{tx},u_1})\mathbf{J}\Big),\end{aligned} \tag{97}$$

$$\begin{aligned}\mathbf{A}^{\nu\mu}_{u_2,u_1} \approx& \mathbf{\Lambda}_{\bar{\mathcal{M}}_{R,u_2}}\Big(\mathbf{D}^{\mu}_{u_2,u_1}\mathbf{\Lambda}_{\text{M}}(\tau_{\text{tx},u_1})\mathbf{J} \\ &+ \mathbf{D}^{\nu}_{u_2,u_1}\mathbf{\Lambda}_{\text{D}}(\tau_{\text{tx},u_1})\mathbf{J}\Big),\end{aligned} \tag{98}$$

$$\begin{aligned}\mathbf{A}^{\mu\nu}_{u_2,u_1} \approx& \mathbf{\Lambda}_{\bar{\mathcal{N}}_{R,u_2}}\Big(\mathbf{J}\mathbf{D}^{\mu*}_{u_2,u_1}\mathbf{\Lambda}^*_{\text{D}}(\tau_{\text{tx},u_1}) \\ &+ \mathbf{J}\mathbf{D}^{\nu*}_{u_2,u_1}\mathbf{\Lambda}^*_{\text{M}}(\tau_{\text{tx},u_1})\mathbf{J}\Big).\end{aligned} \tag{99}$$

From (90), we know that $D_{u_2,u_1,v_1}[n,l]$ is negligible if n is not around l. Consequently, this characteristic applies to $D^{\mu}_{u_2,u_1}[n,l]$ and $D^{\nu}_{u_2,u_1}[n,l]$. This renders that dominant terms of $\mathbf{A}^{\mu\mu}_{u_2,u_1}$ and $A^{\nu\mu}_{u_2,u_1}[n,l]$ are around their diagonal while those of $\mathbf{A}^{\nu\mu}_{u_2,u_1}$ and $\mathbf{A}^{\mu\nu}_{u_2,u_1}$ are around their anti-diagonal; other terms are insignificant. Define

$$\breve{\mathbf{C}}_{u_1} \triangleq \mathbf{\Lambda}_{\text{D}}(\tau_{\text{tx},u_1})\mathbf{C}_{u_1} + \mathbf{\Lambda}_{\text{M}}(\tau_{\text{tx},u_1})\mathbf{J}\mathbf{C}^*_{u_1}, \tag{100}$$

$$\breve{\mathbf{R}}_{u_2} \triangleq \sum_{u_1=1}^{U_T}\mathbf{D}^{\mu}_{u_2,u_1}\breve{\mathbf{C}}_{u_1} + \mathbf{D}^{\nu}_{u_2,u_1}\mathbf{J}\breve{\mathbf{C}}^*_{u_1}, \tag{101}$$

$$\hat{\mathbf{R}}_{u_2} \triangleq \mathbf{\Lambda}_{\mu_{R,u_2}}\breve{\mathbf{R}}_{u_2} + \mathbf{\Lambda}_{\nu_{R,u_2}}\mathbf{J}\breve{\mathbf{R}}^*_{u_2}, \tag{102}$$

and successively substitute them. Next, substitute (96), (97), (98), and (99) into (28). Then, after appropriate re-arranging the terms in the resulting lengthy equation, we obtain

$$\breve{\mathbf{Y}}_{u_2} \approx \mathbf{\Lambda}_{\text{D}}(\tau_{\text{rx},u_2})\hat{\mathbf{R}}_{u_2} + \mathbf{\Lambda}_{\text{M}}(\tau_{\text{rx},u_2})\mathbf{J}\hat{\mathbf{R}}^*_{u_2} + \breve{\boldsymbol{\eta}}_{u_2}. \tag{103}$$

From (101), (102), (39), (39), we can also express

$$\hat{\mathbf{R}}_{u_2} = \mathbf{B}^{D}_{u_2,u_1}\breve{\mathbf{C}}_{u_1} + \mathbf{B}^{M}_{u_2,u_1}\breve{\mathbf{C}}^*_{u_1}. \tag{104}$$

Next, we convert (100), (104), and (103) into the real-valued matrix form and obtain

$$[\breve{\mathbf{C}}_{u_1}]_{\text{RI}} = \mathbf{\Lambda}_{\text{tx},u_1}[\mathbf{C}_{u_1}]_{\text{RI}}, \tag{105}$$

$$[\hat{\mathbf{R}}_{u_2}]_{\text{RI}} = \sum_{u_1=1}^{U_T}\bar{\mathbf{Q}}_{u_2,u_1}[\breve{\mathbf{C}}_{u_1}]_{\text{RI}}, \tag{106}$$

$$[\breve{\mathbf{Y}}_{u_2}]_{\text{RI}} = \mathbf{\Lambda}_{\text{rx},u_2}[\hat{\mathbf{R}}_{u_2}]_{\text{RI}} + [\breve{\boldsymbol{\eta}}_{u_2}]_{\text{RI}}. \tag{107}$$

Substituting the above equations successively gives (42).

This article has been accepted for publication in a future issue of this journal, but has not been fully edited. Content may change prior to final publication. Citation information: DOI 10.1109/TWC.2017.2696947, IEEE Transactions on Wireless Communications

$$A^{\mu\mu}_{u_2,u_1}[n,l] = \sum_{v_1=1}^{V_T} e^{j\theta_{T,u_1,v_1}} \Big[\Big(\Big\{\Big[H^{u_2}_{u_1,v_1}(f)\Big\{[G_T(f)\gamma_T(f-l\Delta f)\bar{\mathcal{M}}_{T,u_1,v_1}(f)] * \Psi_{T,u_1}(f)\Big\}\Big] * \Psi_{R,u_2}(f+\alpha_{u_2})\Big\} G_R(f) e^{j2\pi f t_0}\bar{\mathcal{M}}_{R,u_2}(f)\Big) * \gamma_R(f)\Big]_{f=f_n}, \quad (80)$$

$$A^{\nu\nu}_{u_2,u_1}[n,l] = \sum_{v_1=1}^{V_T} e^{-j\theta_{T,u_1,v_1}} \Big[\Big(\Big\{\Big[H^{u_2*}_{u_1,v_1}(-f)\Big\{[G_T(f)\gamma_T(f-l\Delta f)\bar{\mathcal{N}}^*_{T,u_1,v_1}(-f)] * \Psi^*_{T,u_1}(-f)\Big\}\Big] * \Psi^*_{R,u_2}(-f+\alpha_{u_2})\Big\} G^*_R(-f) e^{j2\pi f t_0}\bar{\mathcal{N}}_{R,u_2}(f)\Big) * \gamma_R(f)\Big]_{f=f_n}, \quad (81)$$

$$A^{\nu\mu}_{u_2,u_1}[n,l] = \sum_{v_1=1}^{V_T} e^{j\theta_{T,u_1,v_1}} \Big[\Big(\Big\{\Big[H^{u_2}_{u_1,v_1}(f)\Big\{[G^*_T(-f)\gamma^*_T(-f-l\Delta f)\bar{\mathcal{N}}_{T,u_1,v_1}(f)] * \Psi_{T,u_1}(f)\Big\}\Big] * \Psi_{R,u_2}(f+\alpha_{u_2})\Big\} G^*_R(-f) e^{j2\pi f t_0}\bar{\mathcal{M}}_{R,u_2}(f)\Big) * \gamma_R(f)\Big]_{f=f_n}, \quad (82)$$

$$A^{\mu\nu}_{u_2,u_1}[n,l] = \sum_{v_1=1}^{V_T} e^{-j\theta_{T,u_1,v_1}} \Big[\Big(\Big\{\Big[H^{u_2*}_{u_1,v_1}(-f)\Big\{[G^*_T(-f)\gamma^*_T(-f-l\Delta f)\bar{\mathcal{M}}^*_{T,u_1,v_1}(-f)] * \Psi^*_{T,u_1}(-f)\Big\}\Big] * \Psi^*_{R,u_2}(-f+\alpha_{u_2})\Big\} G^*_R(-f) e^{j2\pi f t_0}\bar{\mathcal{N}}_{R,u_2}(f)\Big) * \gamma_R(f)\Big]_{f=f_n}, \quad (83)$$

$$\breve{\eta}_{u_2}[n] = \Big[\Big\{[W_{u_2}(f) * \Psi_{R,u_2}(f+\alpha_{u_2})]G_R(f)\bar{\mu}_{R,u_2}(f)e^{j2\pi f t_0} + [W^*_{u_2}(-f) * \Psi^*_{R,u_2}(-f+\alpha_{u_2})]G_R(f)e^{j2\pi f t_0}\bar{\nu}_{R,u_2}(f)\Big\} * \gamma_R(f)\Big]_{f=f_n}. \quad (84)$$

$$A^{\mu\mu}_{u_2,u_1}[n,l] \approx \sum_{v_1=1}^{V_T} e^{j\theta_{T,u_1,v_1}} \Big[\Big(\Big\{\Big[H^{u_2}_{u_1,v_1}(f)\Big\{[G_T(f)\gamma_T(f-l\Delta f)\bar{\mathcal{M}}_{T,u_1,v_1}[l]] * \Psi_{T,u_1}(f)\Big\}\Big] * \Psi_{R,u_2}(f+\alpha_{u_2})\Big\} G_R(f) e^{j2\pi f t_0}\bar{\mathcal{M}}_{R,u_2}[n]\Big) * \gamma_R(f)\Big]_{f=f_n}$$
$$= \frac{\bar{\mathcal{M}}_{R,u_2}[n]}{2}\Big[(1+e^{-j2\pi f_l \tau_{\mathrm{tx},u_1}})D^{\mu}_{u_2,u_1}[n,l] + (1-e^{-j2\pi f_l \tau_{\mathrm{tx},u_1}})D^{\nu}_{u_2,u_1}[n,l]\Big] \quad (89)$$

$$D_{u_2,u_1,v_1}[n,l] \triangleq \Big[\Big\{\Big[\Big(\{[\gamma_T(f-l\Delta f)G_T(f)] * \Psi_{T,u_1}(f)\}H^{u_2}_{u_1,v_1}(f)\Big) * \Psi_{R,u_2}(f+\alpha_{u_2})\Big] G_R(f) e^{j2\pi f t_0}\Big\} * \gamma_R(f)\Big]_{f=f_n} \quad (90)$$

$$A^{\nu\nu}_{u_2,u_1}[n,l] \approx \frac{\bar{\mathcal{N}}_{R,u_2}[n]}{2}\Big[(1-e^{-j2\pi f_l \tau_{\mathrm{tx},u_1}})D^{\mu*}_{u_2,u_1}[-n,-l] + (1+e^{-j2\pi f_l \tau_{\mathrm{tx},u_1}})D^{\nu*}_{u_2,u_1}[-n,-l]\Big] \quad (93)$$

$$A^{\nu\mu}_{u_2,u_1}[n,l] \approx \frac{\bar{\mathcal{M}}_{R,u_2}[n]}{2}\Big[(1-e^{j2\pi f_l \tau_{\mathrm{tx},u_1}})D^{\mu}_{u_2,u_1}[n,-l] + (1+e^{j2\pi f_l \tau_{\mathrm{tx},u_1}})D^{\nu}_{u_2,u_1}[n,-l]\Big] \quad (94)$$

$$A^{\mu\nu}_{u_2,u_1}[n,l] \approx \frac{\bar{\mathcal{N}}_{R,u_2}[n]}{2}\Big[(1+e^{j2\pi f_l \tau_{\mathrm{tx},u_1}})D^{\mu*}_{u_2,u_1}[-n,l] + (1-e^{j2\pi f_l \tau_{\mathrm{tx},u_1}})D^{\nu*}_{u_2,u_1}[-n,l]\Big] \quad (95)$$

Next, we present development for the expression of ξ_n in (48). From (46) and (47), we have

$$\xi_n \approx \frac{\mathbf{A}^{\nu\mu}_{u_2,u_1}[-n,n] + \mathbf{A}^{\mu\nu}_{u_2,u_1}[-n,n]}{\mathbf{A}^{\mu\mu}_{u_2,u_1}[n,n]}. \quad (108)$$

Since $\mathcal{M}_{T,u_1,v_1}[n] \gg \mathcal{N}_{T,u_1,v_1}[n]$, from (89), we have

$$\mathbf{A}^{\mu\mu}_{u_2,u_1}[n,n] \approx 0.5\bar{\mathcal{M}}_{R,u_2}[n](1+e^{-j2\pi f_n \tau_{\mathrm{tx},u_1}})D^{\mu}_{u_2,u_1}[n,n]. \quad (109)$$

Similarly, since $\mathcal{M}_{R,u_2}[n] \gg \mathcal{N}^*_{R,u_2}[-n]$, we have $\bar{\mathcal{M}}_{R,u_2}[n] \approx 0.5\mathcal{M}_{R,u_2}[n](1+e^{-j2\pi f_n \tau_{\mathrm{rx},u_2}})$. Then, we obtain $\bar{\mathcal{M}}_{R,u_2}[-n]/\bar{\mathcal{M}}^*_{R,u_2}[n] \approx \mathcal{M}_{R,u_2}[-n]/\mathcal{M}^*_{R,u_2}[n]$ and $\bar{\mathcal{N}}_{R,u_2}[-n]/\bar{\mathcal{M}}^*_{R,u_2}[n] \approx \mathcal{N}_{R,u_2}[-n]/\mathcal{M}^*_{R,u_2}[n] + \frac{1-e^{j2\pi f_n \tau_{\mathrm{rx},u_2}}}{1+e^{j2\pi f_n \tau_{\mathrm{rx},u_2}}}$. By substituting (94), (95), and (109) into (108) and applying the above approximations, we obtain (48).

REFERENCES

[1] S. Rangan, T. S. Rappaport, and E. Erkip, "Millimeter-wave cellular wireless networks: Potentials and challenges," *Proc. IEEE*, vol. 102, no. 3, pp. 366–385, Mar. 2014.

[2] T. S. Rappaport, S. Sun, R. Mayzus, H. Zhao, Y. Azar, K. Wang, G. N. Wong, J. K. Schulz, M. Samimi and F. Gutierrez, "Millimeter wave mobile communications for 5G cellular: It will work!," *IEEE Access*, vol.1, pp. 335–349, May 2013.

[3] Z. Pi and F. Khan, "An introduction to millimeter-wave mobile broadband systems," *IEEE* Commun. Mag., vol.49, no. 6, pp. 101–107, Jun. 2011.

[4] M. Valkama, M. Renfors, and V. Koivunen, "Compensation of frequency-selective I/Q imbalances in wideband receivers: Models and algorithms," in *Proc. IEEE SPAWC*, Mar. 2001, pp. 42–45.

[5] L. Anttila, M. Valkama, and M. Renfors, "Blind compensation of frequency-selective I/Q imbalances in quadrature radio receivers: Circularity-based approach," *IEEE ICASSP*, 2007, pp. III-245–248.

[6] L. Anttila, M. Valkama, and M. Renfors, "Circularity-based I/Q imbalance compensation in wideband direct-conversion receivers," *IEEE Trans. Veh. Tech.*, vol. 57, no. 4, pp. 2099–2113, 2008.

[7] L. Anttila, M. Valkama, and M. Renfors, "Frequency-selective I/Q mismatch calibration of wideband direct-conversion transmitters," *IEEE*

Trans. Circuits Syst. II, Exp. Briefs, vol. 55, no. 4, pp. 359–363, May 2008.

[8] Y. Yoshida, K. Hayashi, H. Sakai, W. Bocquet, "Analysis and compensation of transmitter IQ imbalances in OFDMA and SC-FDMA systems," *IEEE Trans. Signal Process*, vol. 57, no. 8, pp. 3119–3129, Aug. 2009.

[9] A. Hakkarainen, J. Werner, K. R. Dandekar, and M. Valkama, "Analysis and augmented spatial processing for uplink OFDMA MU-MIMO receiver with transceiver I/Q imbalance and external interference," *IEEE Trans. Wireless Commun.*, vol. 15, no. 5, pp. 3422–3439, May 2016.

[10] A. Tarighat, R. Bagheri, and A. H. Sayed, "Compensation schemes and performance analysis of IQ imbalances in OFDM receivers," *IEEE Trans. Signal Process.*, vol. 53, no. 8, pp. 3257–3268, Aug. 2005.

[11] B. Narasimhan, D. Wang, S. Narayanan, H. Minn, and N. Al-Dhahir, "Digital compensation of frequency-dependent joint Tx/Rx I/Q imbalance in OFDM systems under high mobility," *IEEE J. Select. Topics Signal Process.*, vol. 3, no. 3, pp. 405–417, Jun. 2009.

[12] Y. Li, L. Fan, H. Lin, and M. Zhao, "A new method to simultaneously estimate TX/RX IQ imbalance and channel for OFDM systems," in *IEEE ICC*, June 2013, pp. 4551–4555.

[13] W. Kirkland and K. Teo, "I/Q distortion correction for OFDM direct conversion receiver," *Electron. Lett*, vol. 39, no. 1, pp. 131–133, 2003.

[14] L. Brötje, S. Vogeler, K.-D. Kammeyer, R. Rückriem, and S. Fechtel, "Estimation and correction of transmitter-caused I/Q imbalance in OFDM systems," in *Intl. OFDM Workshop*, Sept. 2002, pp. 178–182.

[15] Y. Egashira, Y. Tanabe, and K. Sato, "A novel IQ imbalance compensation method with pilot-signals for OFDM system," in *IEEE VTC*, Sept. 2006.

[16] H. Minn and D. Munoz, "Pilot designs for channel estimation of MIMO OFDM systems with frequency-dependent I/Q imbalances", *IEEE Trans. Commun.*,, vol. 58, no. 8, pp. 2252–2264, Aug. 2010.

[17] A. Khansefid, H. Minn, N. Al-Dhahir, H. Huang, and X. Du, "Pilot designs and compensation scheme for severe RF distortions in millimeter-wave massive MIMO systems," in *IEEE Globecom MCHFB Workshop*, 2016.

[18] P. Rabiei, W. Namgoong, and N. Al-Dhahir, "Reduced-complexity joint baseband compensation of phase noise and I/Q imbalance for MIMO-OFDM systems," *IEEE Trans. Wireless Commun.*, vol. 9, no. 11, pp. 3450–3460, Nov. 2010.

[19] Q. Zou, A. Tarighat, and A. H. Sayed, "Joint compensation of IQ imbalance and phase noise in OFDM wireless systems," *IEEE Trans. Commun.*, vol. 57, no. 2, pp. 404–414, Feb. 2009.

[20] H. Huang, W. G. Wang, and J. He, "Phase noise and frequency offset compensation in high frequency MIMO-OFDM system," in *IEEE ICC*, June 2015, pp. 1280–1285.

[21] H. Yang, W. J. Shin, S. Lee and Y. H. You, "A robust estimation of residual carrier frequency offset with I/Q imbalance in OFDM systems," *IEEE Trans. Veh. Technol.*, vol. 64, no. 3, pp. 1254–1259, Mar. 2015.

[22] C. Zhang, Z. Xiao, B. Gao, L. Su and D. Jin, "Three-stage treatment of TX/RX IQ imbalance and channel with CFO for SC-FDE systems," *IEEE Commun. Lett.*, vol. 18, no. 2, pp. 297–300, Feb. 2014.

[23] S. Krone and G. Fettweis, "Capacity analysis for OFDM systems with transceiver I/Q imbalance," *in Proc. 2008 IEEE GLOBECOM*, pp. 16.

[24] P. Mathecken, T. Riihonen, S. Werner, and R. Wichman, "Performance analysis of OFDM with Wiener phase noise and frequency selective fading channel," *IEEE Trans. Commun.*, vol. 59, pp. 1321–1331, May 2011.

[25] V. K. V. Gottumukkala and H. Minn, "Capacity analysis and pilot-data power allocation for MIMO-OFDM with transmitter and receiver IQ imbalances and residual carrier frequency offset," *IEEE Trans. Veh. Technol.*, vol. 61, no. 2, pp. 553–565, Feb. 2012.

[26] A. Gokceoglu, et al., "Mutual information analysis of OFDM radio link under phase noise, IQ imbalance and frequency-selective fading channel," *IEEE Trans. Wireless Commun.*, vol. 12, no. 6, pp. 3048–3059, Jun. 2013.

[27] W. C. Lai, Y. T. Liao and T. Y. Hsu, "A cost-effective preamble-assisted engine with skew calibrator for frequency-dependent I/Q imbalance in 4x4 MIMO-OFDM modem," *IEEE Trans. Circuits Syst. I, Reg. Papers*, vol. 60, no. 8, pp. 2199–2212, Aug. 2013.

[28] M. S. Faruk and K. Kikuchi, "Compensation for in-phase/quadrature imbalance in coherent-receiver front end for optical quadrature amplitude modulation," *IEEE Photon. J.*, vol. 5, no. 2, pp. 7800110–7800110, Apr. 2013.

[29] 3GPP, "Study on 3D channel model for LTE (Release 12), 3GPP TR 36.873, v12.2.0," June 2015.

[30] Q. Zhan, H. Minn, N. Al-Dhahir, and H. Huang, "A solution to timing mismatches between the in-phase and quadrature branches of millimeter-wave transmitter and receiver", in *IEEE Globecom MCHFB Workshop*, 2016.

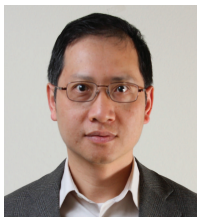

Hlaing Minn (S'99-M'01-SM'07-F'16) received B.E. degree in Electrical Engineering (Electronics) from the Yangon Institute of Technology, Yangon, Myanmar, in 1995; M.Eng. degree in Telecommunications from the Asian Institute of Technology, Pathumthani, Thailand, in 1997; and Ph.D. degree in Electrical Engineering from the University of Victoria, Victoria, BC, Canada, in 2001. During JanuaryAugust 2002, he was a Postdoctoral Fellow with the University of Victoria. He has been with the University of Texas at Dallas since 2002 and is currently a Full Professor. His research interests include wireless communications, statistical signal processing, signal design, cognitive radios, dynamic spectrum access and sharing, next-generation wireless technologies, and wireless health-care technologies.

Dr. Minn serves as an Editor-at-Large since 2016 and served as an Editor from 2005 to 2016 for the IEEE Transactions on Communications. He was also an Editor for International Journal of Communications and Networks from 2008 to 2015. He served as a Technical Program Co-Chair for the Wireless Communications Symposium of the IEEE GLOBECOM 2014 and the Wireless Access Track of the IEEE VTC, Fall 2009, as well as a Technical Program Committee Member for several IEEE conferences.

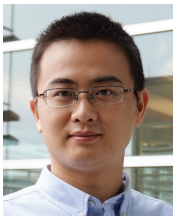

Qi Zhan received the B.E. and M.S. degree in Electrical Engineering from Huazhong University of Science and Technology in 2008 and 2011; and the Ph.D. degree in Electrical Engineering from the University of Texas at Dallas, TX, USA, in 2016. He is currently a senior system engineer with Samsung Semiconductor Inc. at San Diego, CA, USA. His research interests are in the broad areas of wireless communications, signal processing, channel state information and advanced transmission schemes.

Naofal Al-Dhahir (F'08) is Erik Jonsson Distinguished Professor at UT-Dallas. He earned his PhD degree in Electrical Engineering from Stanford University. From 1994 to 2003, he was a principal member of the technical staff at GE Research and AT&T Shannon Laboratory.

He is co-inventor of 41 issued US patents, co-author of over 350 papers and co-recipient of 4 IEEE best paper awards. He is the Editor-in-Chief of IEEE Transactions on Communications.

Huang Huang (S'09-M'11) received the B.Eng. and M.Eng. (Gold medal) degrees from the Harbin Institute of Technology (HIT), Harbin, China, in 2005 and 2007, respectively, and the Ph.D. degree from The Hong Kong University of Science and Technology (HKUST) in 2011. He is currently a Research Engineer with Huawei Technologies Company, Ltd.